Measuring water exchange across the blood-brain barrier using MRI

Ben R Dickie[1], Geoff JM Parker[2,3], Laura M Parkes[1]

1. Division of Neuroscience and Experimental Psychology, University of Manchester, Oxford Road, Manchester, M13 9PT, United Kingdom. 2. Bioxydyn Limited, Manchester, M15 6SZ, United Kingdom. 3. Centre for Medical Image Computing, Department of Computer Science and Department of Neuroinflammation, University College London, London, United Kingdom.

Corresponding author

Email: ben.dickie@manchester.ac.uk

Address: Room 3.07A, Zochonis Building, Brunswick Street, Manchester, M13 9PT

No of pages: 71

No of figures: 4

No of tables: 6

Keywords: blood-brain barrier dysfunction, water permeability, water exchange, magnetic resonance imaging, aquaporin

Abstract

The blood-brain barrier (BBB) regulates the transfer of solutes and essential nutrients into the brain. Growing evidence supports BBB dysfunction in a range of acute and chronic brain diseases, justifying the need for novel research and clinical tools that can non-invasively detect, characterize, and quantify BBB dysfunction *in-vivo*. Many approaches already exist for measuring BBB dysfunction in man using positron emission tomography and magnetic resonance imaging (e.g. dynamic contrast-enhanced-MRI measurements of gadolinium leakage). This review paper focusses on MRI measurements of water exchange across the BBB, which occurs through a wide range of pathways, and is likely to be a highly sensitive

marker of BBB dysfunction. Key mathematical models and acquisition methods are discussed for the two main approaches: those that utilize contrast agents to enhance relaxation rate differences between the intravascular and extravascular compartments and so enhance the sensitivity of MRI signals to BBB water exchange, and those that utilize the dynamic properties of arterial spin labelling to first isolate signal from intravascular spins and then estimate the impact of water exchange on the evolving signal. Data from studies in healthy and pathological brain tissue are discussed, in addition to validation studies in rodents.

Table of Contents

1. Introduction

The blood-brain barrier (BBB) plays a crucial role in the maintenance of neuronal function and health. Its main functions include protecting the brain from blood-borne toxins and pathogens, regulating transport of solutes into the brain, and clearing metabolic waste and other neurotoxic compounds into the bloodstream. In contrast to peripheral tissues, endothelial cells in the brain are sealed together by specialized tight junction proteins. These proteins prevent free paracellular diffusion (i.e. diffusion through gaps between endothelial cells) of particles from the bloodstream into the brain. Furthermore, brain endothelial cells are surrounded by cellular and membrane components including pericytes, basement membrane, perivascular channels, and astrocyte endfeet, each forming additional physical barriers to diffusion [1–3] (Figure 1). Solutes required by the brain for cellular metabolism, repair, and maintenance, cross the BBB through specialized proteins located on endothelial cell membranes. Rapid transcellular diffusion across the endothelial cell membrane itself is possible only for lipid-soluble substances such as non-polar molecular gases (e.g. O_2 and CO_2) and low molecular weight alcohols (e.g. ethanol, butanol).

Blood-brain barrier dysfunction occurs in many conditions including ageing, stroke, cancer, multiple sclerosis, and neurodegeneration, and often occurs concomitantly with neuro-inflammation. Non-invasive methods to probe BBB dysfunction *in-vivo* are needed to understand the impact of these alterations on the pathogenesis and progression of these conditions. Most current approaches aim to use imaging methods to track the uptake of intravenously injected tracers as they pass from the blood stream into the brain. In animal models, 2-photon microscopy can monitor leakage of fluorescent dyes across the BBB, but the field of view is small, and scanning depth is limited to a few millimetres below the cortical surface. Photoacoustic imaging can bridge the gap between microscopic and macroscopic scales, enabling imaging of dyes or probes with specific absorption characteristics (e.g.

Evans blue) at greater depths than fluorescence based imaging systems [4], but still does not have adequate penetration for human brain use, and is challenging to quantify. Positron emission tomography (PET) and magnetic resonance imaging (MRI) have lower spatial resolution, but can image the entire brain using quantitative methods, enabling regional assessment. Importantly, they can be applied to humans, as well as rodents.

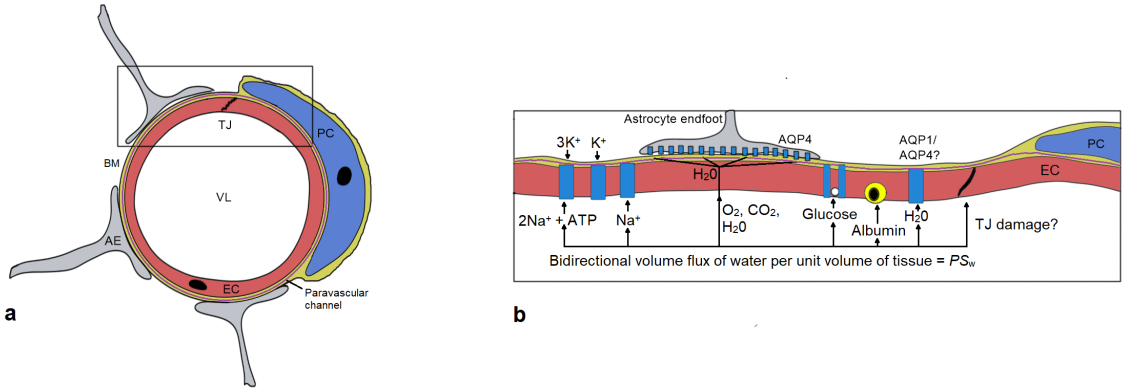

Figure 1. The blood-brain barrier (BBB). **a** The vessel lumen (VL) is formed by endothelial cells (EC) sealed together by tight junction (TJ) proteins. Surrounding the ECs is a basement membrane composed of extracellular matrix proteins including laminin, fibrin, and collagen. Paravascular pathways of the glymphatic system are embedded within this membrane. Astrocyte endfeet (AE) and pericytes (PC) surround the ECs and play crucial roles in neurovascular coupling, as well as forming physical barriers to diffusion across the BBB. **b** An enlarged diagram of the blood-brain interface from the box in **a**. Long-term preservation of an optimal ionic and nutrient-rich environment for synaptic and neural function is achieved by specific ion channels and transporters. Ion channels facilitate passive diffusion of K^+ and Na^+ ions along electrochemical gradients. Ion pumps actively transport ions against an electrochemical gradient (e.g., the Na^+-K^+-ATPase ion pump) and work in combination with ion channels to maintain trans-endothelial ion concentration differences. Gases (in particular O_2, CO_2) and other lipophilic substances diffuse freely across the endothelial cell membranes. Diffusion of water also occurs across the endothelial membrane, but is very slow in comparison. Larger hydrophilic solutes required for brain functioning (i.e., metabolites, vitamins, nucleotides, simple sugars) pass through specialized proteins located on the luminal and abluminal cell membranes which act to accelerate delivery. Simple sugars such as glucose are transported into the brain by specialized carrier-mediated proteins such as GLUT1. Large circulating proteins (e.g. albumin, insulin) and polysaccharides, which are often of greater dimensions than transmembrane channels and transporters themselves, pass across the BBB by receptor mediated transcytosis. Carrier and receptor mediated transport are restricted to the specific molecules they are encoded for. Tight junction proteins seal the endothelial cells together but this location between cells may provide a route for passive diffusion of molecules into the brain if the proteins are damaged or expression downregulated. Water movement can occur through all these pathways, and possibly through dedicated aquaporin channels located on the endothelial cells (AQP1/AQP4). Water transfer therefore has the potential to be altered in a range of BBB pathologies. In this diagram, all transmembrane proteins have been depicted as bridging the luminal-abluminal gap entirely; however, in reality these proteins exist on luminal and/or luminal membranes and transport solutes into and out of the endothelial cell itself. Together luminal and abluminal proteins act to move solutes from blood to brain or vice- versa.

PET has the potential to provide highly specific information on the activity of BBB transporters (e.g. GLUT1 using ^{18}F-Fluro-2-deoxy-2-D-glucose [5] or P-gp using [^{11}C]verapamil [6]). Accurate quantification requires arterial or venous blood sampling, and repeat scanning in at-risk healthy populations (e.g. for longitudinal ageing and dementia studies) is difficult to justify due to cumulative doses of ionising radiation. MRI has the potential to spatially map BBB transporter function due to recent advances in molecular imaging sequences (e.g. chemical-exchange saturation transfer imaging). However, these methods are still in their infancy and lack validation [7].

MRI measurements in clinical use are currently limited to measuring paracellular leakage of low molecular weight gadolinium contrast agents. Unfortunately, these tracers are not specifically designed to probe BBB function, are thought to cross the BBB via paracellular routes only, and leak very slowly unless damage to the tight junctions or endothelial cell membrane is severe. While this is useful to help differentiate severely disrupted from healthy BBB, e.g. in stroke or oncology, these tracers are not well suited for identifying abnormal tissue in pathologies where BBB breakdown is more subtle (e.g. that due to ageing and neurodegenerative diseases), or where dysfunction alters the activity of specific transporters through which the contrast agent does not pass. Due to the low amplitude of signal change detected using these methods, factors such as partial volume errors, Gibbs ringing, signal drift, patient motion, arterial input function definition errors, and kinetic model inaccuracy can confound measurements [8–10]. It is also possible that such tracers do not leak across the BBB at all until paracellular pores reach a certain size [11,12].

While it has long been recognised that water does not diffuse freely across the BBB [13–18], the idea that water could be used to probe BBB function has only recently been proposed. Recent interest in novel approaches to probe BBB water permeability have been triggered by safety concerns relating to accumulation of gadolinium contrast media in the brain, in addition to a desire to find more sensitive approaches for studying subtle BBB alterations. In

addition to potential safety benefits, the use of water to study BBB function has the following key differences compared to other tracers:

1. At equilibrium in the healthy brain, water is transported across the BBB by both passive (diffusive) and active mechanisms (through co-transporters and uniporters) [19], potentially providing sensitivity to a wide range of BBB pathologies.
2. Due to the small size of a water molecule, changes that affect diffusive permeability of the BBB are likely to be detectable at an earlier stage of disease, when damage is more subtle.
3. Water has its own transport protein (aquaporins), which cannot be probed using other tracers.

A number of MRI techniques to measure BBB water exchange have been proposed. These can be grouped primarily into those that utilise an exogenous contrast agent (e.g. contrast-enhanced MRI) and those that do not (e.g. arterial spin labelling (ASL) MRI). This review summarises evidence for limited water exchange across the BBB, discusses theory and modelling relevant for MRI BBB water exchange measurements; and discusses MRI methods for measuring BBB water exchange, including their limitations, technical and biological validation, and applications to healthy and diseased brain tissue.

2. Evidence for limited BBB water exchange

If a molecule has very high BBB permeability, the fraction of these molecules that pass across the BBB ('extraction fraction'), either by passive diffusion or active transport, during a single pass will be close to 1. This is because, as the permeability of the barrier to a particular molecule increases, the probability that the molecule will exchange across the barrier before it leaves the capillary bed also increases. In the limit that the permeability is very high relative to the blood velocity, the probability that a particle entering the capillary bed will exchange across the BBB prior to exiting approaches 1.

Extraction fractions (*E*) less than 1 indicate that the molecule is not freely diffusible or rapidly transported, and that barriers (e.g. tight junctions or lack of transporters) limit passage from blood to brain. If cerebral blood flow (CBF; defined as *f)* is also known, then the permeability-surface area product of the BBB to the molecule of interest (*PS*) can also be calculated using the Renkin-Crone equation [20,21]:

$$PS = -\ln(1 - E)\, f \qquad (1)$$

The *PS* product of a molecule in this context describes its flux across the BBB, from blood to brain, and is hence a useful physiological parameter describing the delivery of a molecule to the brain. As its name implies, it is a function of both the permeability of the barrier (*P*) and the surface area of exchange vessels (*S*). *P* will depend on the function and integrity of the blood-brain barrier. *S* depends on the diameter and density of exchange vessels.

Since the 1970's a range of methods to measure the extraction fraction and *PS* of water (PS_w) have been proposed, and applied in rodents and larger mammals, including humans. A summary of key results which inform our current understanding of BBB water transport are given below.

The extraction fraction of water is less than 1 [13–18]. The extraction fraction of water is lower in rodents [14,16,17] than in monkeys [13] and humans [15,18]. This is mainly attributable to inter-species differences in *CBF*, which can be 2-4 greater in rodents than humans. Inter-species variations in extraction do not appear to depend on PS_w [13,16–18,22]. Extraction of water across the BBB decreases with increased arterial CO_2 tension, mainly due to increased *CBF* [13,14,23]. PS_w increases with arterial CO_2 tension, which acts to partially offset the effects of increased *CBF* on extraction [14,17]. Anaesthesia increases extraction fraction, due to large reductions in *CBF*. PS_w also decreases but to a lesser degree [16], indicating that rodent studies that use anaesthesia may underestimate PS_w occurring under normal physiological conditions. *CBF* is regionally correlated with PS_w [18].

3. Definitions of physical parameters governing BBB water exchange

When measuring water exchange across the BBB using MRI, key parameters of interest include volume and magnetisation fluxes, intra- and extravascular magnetisation, intra- and extravascular water population fractions, water exchange rates, and water residence times. The definitions and symbols used for these quantities vary widely between studies, particularly between fields of contrast-enhanced MRI and arterial spin labelling MRI. In this review, we attempt to use consistent nomenclature to bridge the gap between these fields, (Table 1) which we hope will help improve standardisation for future work in this area.

We begin by defining equilibrium and non-equilibrium water exchange kinetics. Equilibrium water exchange describes a system for which the influx and efflux of water across the BBB are equal (i.e., zero net flux). Non-equilibrium or osmotic water exchange is that which leads to unidirectional movement of water (i.e., finite net flux). This review considers measurement of equilibrium BBB water exchange only.

Under equilibrium water exchange conditions, the volume of water moving from blood to brain per unit volume of tissue (also known as the permeability surface area product, $PS_{w,in}$ [mL min^{-1} mL^{-1}]) is by definition equal to the volume flux of water moving from brain to blood ($PS_{w,out}$, [mL min^{-1} mL^{-1}]):

$$PS_{w,in} = PS_{w,out} \tag{2}$$

When placed in an external magnetic field, the magnetic moments associated with each water molecule become preferentially aligned with the field, creating a net bulk longitudinal magnetisation. When fully relaxed (i.e. at equilibrium), the bulk magnetisation in each compartment is proportional to its water content, enabling water population fractions of each compartment to be defined. For a simple two-site exchange system comprising blood and extravascular spaces (Figure 2) the population fractions of water in each of these spaces (p_b [mL mL^{-1}] and p_e [mL mL^{-1}], respectively) are given by:

$$p_b = \frac{M_{0,b}}{M_{0,b} + M_{0,e}} \tag{3}$$

$$p_e = \frac{M_{0,e}}{M_{0,b} + M_{0,e}} \qquad (4)$$

where $M_{0,b}$ and $M_{0,e}$ are the equilibrium longitudinal magnetisations in the blood and extravascular spaces, respectively. Because both water and contrast agent have limited permeability across the endothelial cell membrane itself, we consider water contained within the endothelial cells to be part of the extravascular compartment. The blood compartment is comprised of all water within the vessel lumen, including that within red blood cells and any other non-plasma constituents. The sum of these water population fractions is unity:

$$p_b + p_e = 1 \qquad (5)$$

When longitudinal magnetisation is fully relaxed, the influx and efflux of magnetisation (J; [J] = (magnetisation) min^{-1})) at the BBB are equal and given by:

$$J_{in} = J_{out} \qquad (6)$$

$$k_{in} M_{0,b} = k_{out} M_{0,e} \qquad (7)$$

where k_{in} [min^{-1}] and k_{out} [min^{-1}] are the first-order exchange rate constants governing this exchange. Dividing both sides of equation 7 by the total tissue equilibrium magnetisation $M_{0,t}$ = $M_{0,b}$ + $M_{0,e}$,gives:

$$k_{in} p_b = k_{out} p_e \qquad (8)$$

k_{in} and k_{out} are often expressed as their inverse, the water residence or pre-exchange lifetimes, $\tau_b = 1/k_{in}$ [min] and $\tau_e = 1/ k_{out}$ [min]. These characteristic times describe the mean time spent by each water molecule before exchanging across the BBB.

Equation 8 encapsulates a key property of equilibrium transmembrane water exchange. That is, that while the volume fluxes of water are the same in both directions across the membrane, the rate constants k_{in} and k_{out} are not, unless the water population fractions p_b and p_e are equal. If the volumes of two exchanging compartments are unequal, then the

mean residence time of water molecules in the larger compartment must be smaller to maintain equal bidirectional volume fluxes. Since the blood compartment is smallest, water molecules in the blood compartment must on average exchange across the BBB with a higher probability than water molecules in the extravascular compartment (i.e. $k_{in} > k_{out}$).

The magnetisation influx ($k_{in}M_{0,b}$), can be written in terms of PS_w by dividing by the magnetisation density in blood ($\rho = M_{0,b}/V_b$) and the tissue volume, V_T:

$$PS_w = \frac{k_{in}M_{0,b}}{\rho V_T} = k_{in}\frac{V_b}{V_T} = k_{in}v_b \tag{9}$$

where v_b is the fractional blood volume.

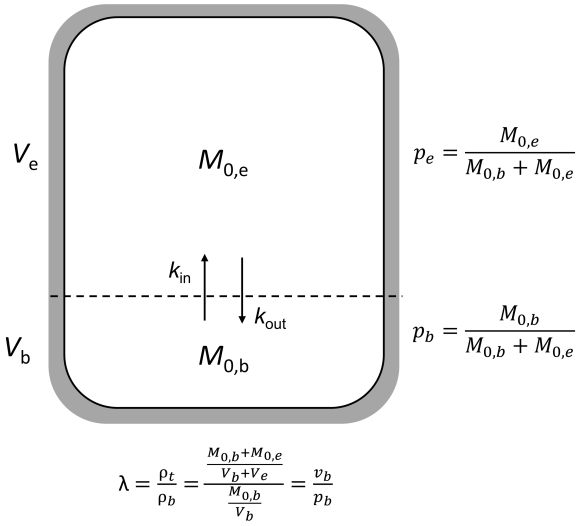

Figure 2. A two-site exchange system consisting of intravascular (bottom) and extravascular (top) spaces with absolute volumes V_b and V_e respectively. The entire volume including both intravascular and extravascular spaces is denoted as 'tissue' throughout this review. Water (magnetisation) exchanges between intravascular and extravascular spaces with rates k_{in} and k_{out}. Flow of magnetisation into and from the intravascular space is ignored for simplicity, but would be required to accurately describe the system in certain applications (e.g. ASL). Both spaces are composed of water-accessible (white) and water-inaccessible volumes (grey). Water-accessible volumes are detectable by MRI and have relative volumes p_b and p_e (= 1- p_b). Water-inaccessible volumes are invisible to MRI, and may differ in size between intravascular and extravascular spaces. The fraction of total equilibrium magnetisation in the intravascular space, p_b, may not therefore necessarily equal the blood volume fraction, v_b. This causes difficulty when calculating parameters that require knowledge of the blood volume, for example the permeability surface area product (PS_w), where the surface area is defined over the blood volume, not the surface area of the water-accessible space. The tissue-blood partition coefficient, λ, describes the ratio of magnetisation density in the entire voxel to that of the intravascular volume, and converts p_b to v_b. Since λ is difficult to measure, it is generally assumed to be invariant across brain regions and subjects. Errors in this assumption will translate directly into errors in PS_w. Estimates of λ are not required to estimate the rate constants k_{in} and k_{out}.

4. The effect of inter-compartmental water exchange on measured relaxation rates and diffusion coefficients

The millimetre spatial resolution of MRI means measured signals are often composed of contributions from multiple distinct microscopic 'water exchanging' compartments. If water exchanges rapidly between these compartments, the compartments themselves are well-mixed, and then observed relaxation rates and diffusion coefficients will appear to arise from a single well mixed compartment (Figure 3a). This is because each water molecule will sample each compartment during the measurement time, and will experience relaxation and diffusion environments that are an average of the multi-compartment system, weighted by their relative volumes. Conversely, if water exchange is slow, water from each individually well-mixed compartment will give rise to distinct signal contributions characterised by the compartmental relaxation and diffusion properties (Figure 3b). For intermediate exchange between compartments, water will experience some averaging effects, but this will not be complete. Each compartment will give rise to distinct signal contributions but these will be dependent on the exchange rate itself (Figure 3c). When measuring BBB water exchange, the primary aim is to quantify the water exchange rates, and possibly water fluxes, between the intra- and extravascular spaces. Ideally, water exchange between sub-compartments of these spaces e.g. between plasma and red-blood cells, or neurones/astrocytes and interstitial fluid, is normally assumed to be fast or the sub-compartments negligibly small, such that a tissue voxel can be treated as a two-site exchange system, instead of a three-, four-, or *N*-site exchange system. In this case, the problem becomes one of distinguishing the amplitudes (i.e., apparent volume fractions) and decay rates (i.e., apparent relaxation rates or apparent diffusivities) of two distinct signal contributions; those arising from intravascular and extravascular compartments. Because the signal decay rates of these contributions depend on the exchange rates and the intrinsic relaxation rates, diffusivities,

and volume fractions of each compartment, the intrinsic relaxation rates or diffusivities of at least one compartment must be measured or known *a priori* to estimate the exchange rates.

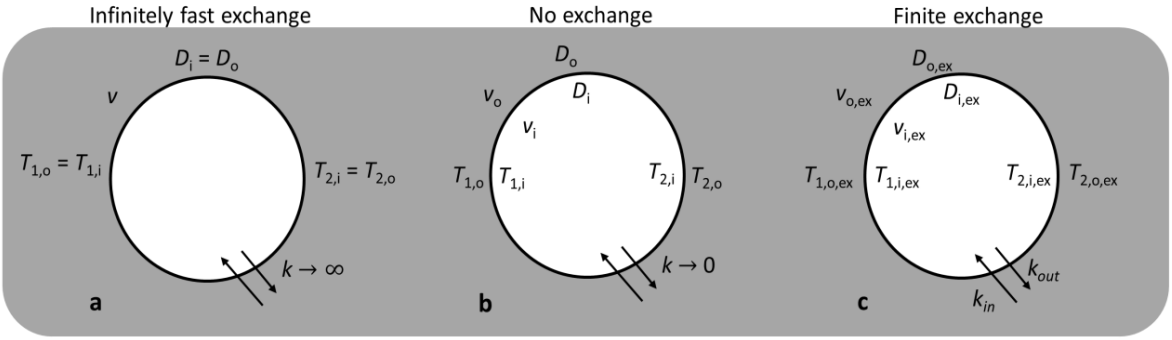

Figure 3. Water exchange across cell membranes. **a** When water exchange across a membrane is very fast, and each compartment is well-mixed, internal and external relaxation rates and diffusion coefficients become averaged together, resulting in a single T_1, T_2 and D for both compartments. Under these conditions the individual compartment volumes cannot be distinguished. **b** When exchange across a membrane is slow or zero, and each compartment is well mixed, water relaxes and diffuses as a multi-component system with intrinsic relaxation times ($T_{1,i}$, $T_{1,o}$, $T_{2,i}$, $T_{2,o}$) and apparent diffusion coefficients (D_o, D_i). If the relaxation rates or diffusivities can be distinguished from one another in the presence of experimental noise, the true volume fractions v_o and v_i can be measured, as these will be determined by the relative magnitudes of the compartmental signal contributions. **c** When exchange across a membrane is finite, water also relaxes and diffuses as a multi-component system. However, the measured relaxation times, diffusion coefficients, and fractional volumes are now dependent on the exchange rates k_{in} and k_{out}.

5. Modelling the effects of BBB water exchange on MRI signals

We have so far described the fundamental physiological properties governing water exchange between intravascular and extravascular compartments, and how these properties affect the nuclear magnetic resonance (NMR) properties of brain tissue. To describe how these properties translate to MRI signal intensities, the temporal (and possibly spatial) evolution of magnetisation in each compartment must be modelled. In all that follows, transcytolemmal water exchange (i.e., water exchange between plasma and red-blood cells, and between interstitial fluid and brain cells) is assumed to be infinitely fast.

The form of the mathematical model used to describe compartmental signal intensities must take into account the experimental method used. To date, available methods can be broadly categorised into contrast agent based, and contrast agent free (e.g. arterial spin labelling) approaches. In contrast agent based approaches, an intravascular contrast agent is

340 introduced into the blood pool to increase intravascular-extravascular T_1 differences.
341 Because T_1 interactions are short range, any changes in the T_1 of the extravascular
342 compartment can be attributed to trans-BBB water exchange. In contrast agent free
343 approaches, arterial spin labelling is used to tag capillary magnetisation, followed by a T_1,
344 T_2, or diffusion-weighted readout, which, because of compartmental differences in T_1, T_2,
345 and D, encodes the compartmentalisation of tagged magnetisation as a function of time. By
346 measuring the location of tagged spins as the label is exchanging, the exchange rate can be
347 determined. The following sections describe the models used to describe MRI signals
348 measured using these methods.

349 *5.1 Exchange models for contrast agent based measurements*

350 Contrast agent based measurements of water exchange were proposed in the 1970s for
351 quantifying water exchange rates across red-blood cells *in-vitro* [24,25]. An extracellular
352 paramagnetic contrast agent (Mn^{2+}) that is unable to cross the red-blood cell membrane was
353 introduced into the plasma of blood, and its effect on intracellular water due to exchange
354 deduced via measurements of T_2. Schwarzbauer et al first adapted this method for *in-vivo*
355 measurements of BBB water exchange [26]. An intravascular contrast agent was introduced
356 into the blood pool via intravenous injection and its effect on the relaxation of extravascular
357 water due to BBB water exchange inferred.

358

359 In the experiments by Schwarzbauer et al. [26] and resulting work that followed [27–31], the
360 effect of exchange was quantified by measuring the effect on T_1, not T_2 as in the earlier red-
361 blood cell studies.

362 Factors other than the exchange rate also contribute to extravascular T_1 and must be
363 accounted for during modelling, including the intrinsic T_1 of the intravascular space (which is
364 now a function of contrast agent concentration), and the blood water population fraction. To
365 distinguish the effects of exchange from these other sources, T_1 relaxation rate

366 measurements must be made for at least 3 contrast agent concentrations (including 0 mM)
367 and in a location containing only blood (e.g. regions of interest in a large artery or vein).

368 The evolution of intravascular and extravascular magnetisation occurring during contrast
369 agent based water exchange measurements can be described using a two-site exchange
370 model via the Bloch McConnell equations [32]:

$$\frac{d}{dt}M_b(t) = \frac{M_{0,b} - M_b(t)}{T_{1,b}} - k_{in}M_b(t) + k_{out}M_e(t) \quad (10)$$

371

$$\frac{d}{dt}M_e(t) = \frac{M_{0,e} - M_e(t)}{T_{1,e}} + k_{in}M_b(t) - k_{out}M_e(t) \quad (11)$$

372

$$M_t(t) = M_b(t) + M_e(t) \quad (12)$$

373 where $M_{0,b}$, $M_{0,e}$, $T_{1,b}$, and $T_{1,e}$ are the equilibrium longitudinal magnetisations and intrinsic
374 T_1 relaxation times for intravascular and extravascular water respectively. k_{in} and k_{out} are the
375 water exchange rate constants into and out of the extravascular space, as defined
376 previously.

377 Solving equations 10-11 for an inversion recovery sequence gives the bi-exponential
378 solution:

$$S = S_0\left[1 - 2(a_s e^{\frac{-TI}{T_{1,S}}} + (1 - a_s)e^{\frac{-TI}{T_{1,L}}})\right] \quad (13)$$

379 where S_0 is the equilibrium signal, a product of water density and scanner calibration factors,
380 TI is the inversion time, and a_s is the apparent (measurable) volume fraction of the short T_1
381 compartment given by:

382

$$a_s = \frac{1}{2} - \frac{1}{2}\left(\frac{\left[\left(\frac{1}{T_{1,e}} - \frac{1}{T_{1,b}}\right)(2p_b - 1) + \ (k_{in} + k_{out})\right]}{\left[\left(\frac{1}{T_{1,e}} - \frac{1}{T_{1,b}} + k_{out} - k_{in}\right)^2 + 4k_{in}k_{out}\right]^{\frac{1}{2}}}\right) \quad (14)$$

383

384 The relaxation rates $1/T_{1,S}$ and $1/T_{1,L}$ are the apparent (observed) T_1 relaxation rates of each
385 compartment, and are given by:

$$\frac{1}{T_{1,S/L}} = \frac{1}{2}\left[\left(\frac{1}{T_{1,e}} + \frac{1}{T_{1,b}} + k_{in} + k_{out}\right) \pm \left[\left(\frac{1}{T_{1,e}} - \frac{1}{T_{1,b}} + k_{out} - k_{in}\right)^2 + 4k_{in}k_{out}\right]^{\frac{1}{2}}\right] \quad (15)$$

386 Inversion recovery measurements of T_1 are time-consuming, which limits brain coverage.
387 Spoiled gradient echo acquisitions (SPGR) are faster enabling full brain coverage, but are
388 more sensitive to transmit B_1 field inhomogeneity. The two-site exchange model for the
389 SPGR sequence is given in [31].

390 Equations 10-11 are functions of time only, and assume that magnetisation is 'well mixed'
391 within each space. If the BBB is damaged and contrast agent extravasates into the
392 interstitial space, interstitial T_1 may decrease sufficiently to drive extravascular T_1 relaxation
393 into a bi-exponential regime (i.e. no longer a single well-mixed compartment). In this case,
394 models that take transcytolemmal water exchange into account may be required to
395 accurately describe the system [33,34]. In the vascular compartment, while the exchange of
396 water between plasma and red blood cells is extremely fast (k ~ 40-80 s^{-1}), large contrast
397 agent concentrations that occur during first pass of a bolus injection may transiently tip
398 relaxation into a bi-exponential regime (for plasma contrast agent concentrations > 10mM, r_1
399 = 3.5-4.5 (mM $s)^{-1}$). Following first pass, the concentration in plasma is much lower (~ 1-2
400 mM) and blood water can be assumed to decay with a single T_1.

Equations 10-11 describe the evolution of intravascular (capillary) and extravascular magnetisation during each TR or inversion recovery period. In 3D SPGR acquisitions, inflow and outflow of magnetisation into and from the capillary bed can be ignored, as by the time of measurement (i.e. acquisition of the centre of k-space), steady state conditions will be met, and inflowing magnetisation will equal that flowing out of the capillary bed. In multislice 2D acquisitions, inflow of partially saturated blood may mean that arterial magnetisation exceeds outflow from the venous compartment. In this case, models should be adapted to account for differences between the amount of magnetisation entering and leaving the capillary bed [35].

5.2 Exchange models for arterial spin-labelling based measurements

Arterial spin labelling (ASL) forms the second major type of MRI acquisition currently used to measure BBB water exchange. In ASL, a perfusion weighted label image is acquired and subtracted from an identical image without label. A post-labelling delay (PLD) time is introduced following the label pulse to allow labelled blood to reach the tissue of interest.

Original ASL models are based on the single compartment Kety model for freely diffusible tracers [36,37]. They incorrectly assume that all labelled water immediately exchanges from capillary to the extravascular space ($PS_w \rightarrow \infty$). Conflicting views exists relating to the importance of this effect in standard ASL acquisitions. Several studies have shown that applying a single compartment model to ASL data can lead to errors of up to 62% in *CBF* [38–40], particularly in white matter where T_1 differences between intra- and extravascular spaces are substantial. Conversely, in rat brain at 9.4T, Carr et al. showed changes in signal intensity caused by typical changes in PS_w were too small to be detectable at the SNR achievable using a standard FAIR sequence of the time [41].

Following these observations, a number of two-compartment models were proposed (Figure 4), and specialized ASL techniques developed to correct CBF estimates for finite PS_w, or to directly quantify the BBB water exchange rate itself. The following sections describe these

two-compartment models and their assumptions; specialist ASL methods for quantifying BBB exchange are discussed in later sections.

Models describing the rate of change of labelled magnetisation in capillary and extravascular spaces were first described by Zhou et al [42] and Parkes et al. [38]:

$$\frac{d}{dt}\Delta M_b(t) = \frac{-\Delta M_b(t)}{T_{1,b}} + \frac{f}{v_b}\cdot\Delta M_a(t) - \frac{f}{v_b}\cdot\Delta M_v(t) - k_{in}\Delta M_b(t) + k_{out}\Delta M_e(t) \qquad (17)$$

$$\frac{d}{dt}\Delta M_e(t) = \frac{-\Delta M_e(t)}{T_{1,e}} + k_{in}\Delta M_b(t) - k_{out}\Delta M_e(t) \qquad (18)$$

$$\Delta M(t) = \Delta M_b(t) + \Delta M_e(t) \qquad (19)$$

where $\Delta M_a(t)$, $\Delta M_v(t)$, $\Delta M_b(t)$, and $\Delta M_e(t)$ are the magnetisation differences between label and control images for the arterial blood, venous blood, capillary blood, and extravascular space respectively, and f is the flow feeding the capillary bed, where [f] = (mL blood) min^{-1} (mL tissue)$^{-1}$. It is worth noting that the exact form of equations 17-19 depend on how the magnetisation and physiological parameters are defined.

The solutions to Eqns 17-18 are known [38], but require knowledge of both ΔM_a and ΔM_v. The arterial magnetisation ΔM_a is defined by the labelling pulse and is therefore approximately known and or can be accurately modelled. However, ΔM_v is typically unknown. Under conditions of infinitely fast exchange, then labels in the capillary and extravascular spaces are assumed to be in equilibrium, and label leaving the voxel will equal that in the extravascular space, weighted by the tissue-blood partition coefficient: $\Delta M_v(t) = \frac{\Delta M_e(t)}{\lambda}$. Under conditions of finite water exchange, ΔM_v and ΔM_e may not be in equilibrium by the time of measurement, or by the time the labelled water begins to leave the tissue. Parkes et al. suggest two possible options for modelling ΔM_v under conditions of finite exchange, termed slow and fast flow approximations [43]. In the slow flow approximation,

which is valid for low perfusion rates (i.e., high extraction fraction, e.g. in human brain), the proportion of label predicted to pass straight into the venous pool will be a small fraction of the total detectable label (1-E = 0.1, where E is the extraction fraction). Furthermore, since the measurement time (post-labelling delay time) will be less than the mean vascular transit time, the label that remains intravascular may not have physically reached the venous pool by the time of measurement. Overall therefore, under conditions of low flow, it is a good assumption that $\Delta M_v \cong 0$. In the fast flow approximation, at higher perfusion rates where extraction of labelled water is lower and vascular transit times are shorter (e.g. in rodents, E ~ 0.7), the proportion of label that remains intravascular and reaches the venous pool may be a significant fraction of the total detectable label. In these circumstances, the transit time of label through the blood compartment will be small and the venous label magnetisation can be approximated by that at the capillary outlet: $\Delta M_v \cong \Delta M_b$.

To simplify the two-compartment exchange model further, Parkes et al. and St Lawrence et al. introduced a zero backflux assumption (k_{out} = 0)[40,44]. This is justified since the extravascular compartment is much larger than the intravascular compartment. For example, assuming a p_b of 0.05 and k_{in} of 3 s^{-1}, k_{out} = 0.16 s^{-1}. At long post-labelling delay times and high PS_w, this assumption may be inaccurate, as most of the label will reside within the extravascular compartment, and efflux of label from the extravascular compartment may equal or be greater than influx, despite low k_{out}. This zero backflux assumption was termed the single pass approximation (SPA), and has also been applied by St. Lawrence et al. to distributed models (see later)[45].

Alsop et al. [46] proposed an alternative two-compartment model for describing ASL signals, but did not explicitly describe its use for quantifying trans-BBB exchange at the time. This model used the existing architecture of the one-compartment Kety ‘tissue’ model [36,37], but added an ‘adhoc’ arterial and capillary compartment. By defining an arterial transit time (δ_a; the transit time from the labelling position to the voxel), and tissue transit time (δ; the transit time from the labelling position to the extravascular space), the two model components were

linked by assuming that the BBB simply slows the delivery of label from the vasculature to the blood. As in the original Kety model, all labelled water exchanges into the tissue, and is simply delayed in getting there by a time: $T_{ex} = \delta - \delta_a$. Venous outflow is treated in the same manner as the Kety model, assuming venous label is instantaneously equilibrated with the extravascular label. This latter assumption requires infinitely fast water exchange, contradicting the prior assumption of finite exchange time T_{ex}. It is unclear how this will affect accuracy of T_{ex} estimates, but may be significant at high flow rates (i.e. in rodents).

Equations 17-18 describe the evolution of longitudinal magnetisation. However, ASL signal is also weighted by transverse relaxation (T_2), due to the moderate echo times used. Wells et al. showed the T_2 of labelled water changes with post-labelling delay time [47], indicating that the T_2 values of water in vascular and extravascular compartments differ, and could impact the accuracy of water exchange measurements in methods that do not account for compartmental T_2 differences. Based on these findings, Gregori et al. adapted the Alsop et al. model [48] to account for differences in both T_1 and T_2.

The models of Zhou et al., Parkes et al., Gregori et al. and Alsop et al. described above assume the label is well-mixed within both the capillary and extravascular spaces. In reality labelled blood water is progressively extracted as it passes through the capillary bed. The tissue homogeneity model first proposed by Johnson and Wilson models the label concentration as a function of both time and position along the capillary bed, and the extravascular space as function of time only (i.e., compartment assumption), but has no closed form solution [49]. In 1998, St Lawrence et al. proposed an adiabatic approximation to the homogeneity model, which provides a time-domain solution by assuming the rate of change of label in the extravascular compartment is much slower than that in the vascular compartment [50] , which can be justified when considering the much larger relative volume of the extravascular space.

A potential inaccuracy with many of the proposed models is that they assume that the labelled water is available to exchange immediately as it reaches the tissue. This may not be

true, as water may traverse vessels that have a lower exchange rate (e.g. arterioles) before it enters the capillary bed. To account for this additional delay, Li et al. added an additional pre-capillary compartment with associated transit time t_{ex} to a standard tissue homogeneity model [51]. Applying the model to healthy human brain tissue, a mean delay time t_{ex} of 0.51 s seconds was observed, suggesting water does not begin to exchange immediately once it has entered the voxel.

Table 1. Parameter definitions

CBF	Cerebral blood flow	mL (blood) mL (tissue)$^{-1}$ min^{-1}
k_{in}	Exchange rate of water from blood to	min^{-1}
k_{out}	Exchange rate of water from brain to	min^{-1}
J	Unidirectional magnetisation flux	(magnetisation) min^{-1}
PS_w	Permeability surface-area product to water	mL (blood or extravascular fluid) mL(tissue)$^{-1}$ min^{-1}
E	Extraction fraction	Fraction of blood water extracted in a single pass
τ_b	Mean blood water residence time	s
T_{ex}	Pre-exchange lifetime (=τ_b)	s
δ	Tissue transit time	s
δ_a	Arterial transit time	s
τ_e	Mean extravascular residence time	s
V_b	Absolute blood volume	mL
V_e	Absolute extravascular volume	mL
V_T	Absolute voxel volume	mL
v_b	Fractional blood volume	(mL blood) (mL tissue)$^{-1}$
v_e	Fractional interstitial volume	(mL extravascular space) (mL tissue)$^{-1}$
p_b	Blood water population fraction	(mL blood water) (mL blood + extravascular water)$^{-1}$
p_e	Extravascular water population	(mL extravascular water) (mL blood + extravascular water)$^{-1}$
λ	Brain-blood partition coefficient	Magnetic moment (mL tissue)$^{-1}$/ magnetic moment (mL blood)$^{-1}$
M_t	Total voxel magnetisation	Magnetic moment per unit volume of tissue
M_b	Blood magnetisation	Magnetic moment per unit volume of blood
M_e	Extravascular magnetisation	Magnetic moment per unit volume of extravascular space
$M_{0,b}$	Equilibrium blood magnetisation	Magnetic moment per unit volume of blood
$M_{0,e}$	Equilibrium extravascular magnetisation density	Magnetic moment per unit volume of extravascular space

6. MRI approaches for quantifying BBB water exchange

There are currently two main MRI approaches for measuring BBB water exchange, those that use a contrast agent, and those that do not (contrast agent free). Contrast agent based approaches utilize the relaxation effects of injectable paramagnetic contrast agents to shorten the T_1 relaxation rate of water in blood relative to water in the extravascular space,

pushing longitudinal relaxation of voxel water from a mono-exponential (in the limit of infinitely fast exchange between compartments) to an exchange-dependent bi-exponential regime. Contrast agent free approaches generally employ arterial spin labelling MRI (usually in combination with T_2- or diffusion-weighting) to track exchange of labelled water as it passes from blood to brain. In either case, the critical challenge lies in precisely and accurately distinguishing components of signal arising from intravascular and extravascular water.

The following sections summarize methods proposed to date for measuring BBB water exchange, and provide discussion of their main assumptions and limitations. Hybrid approaches that combine contrast agents with ASL, in addition to a number of more recent approaches, are also discussed. All methods are summarised in Table 3.

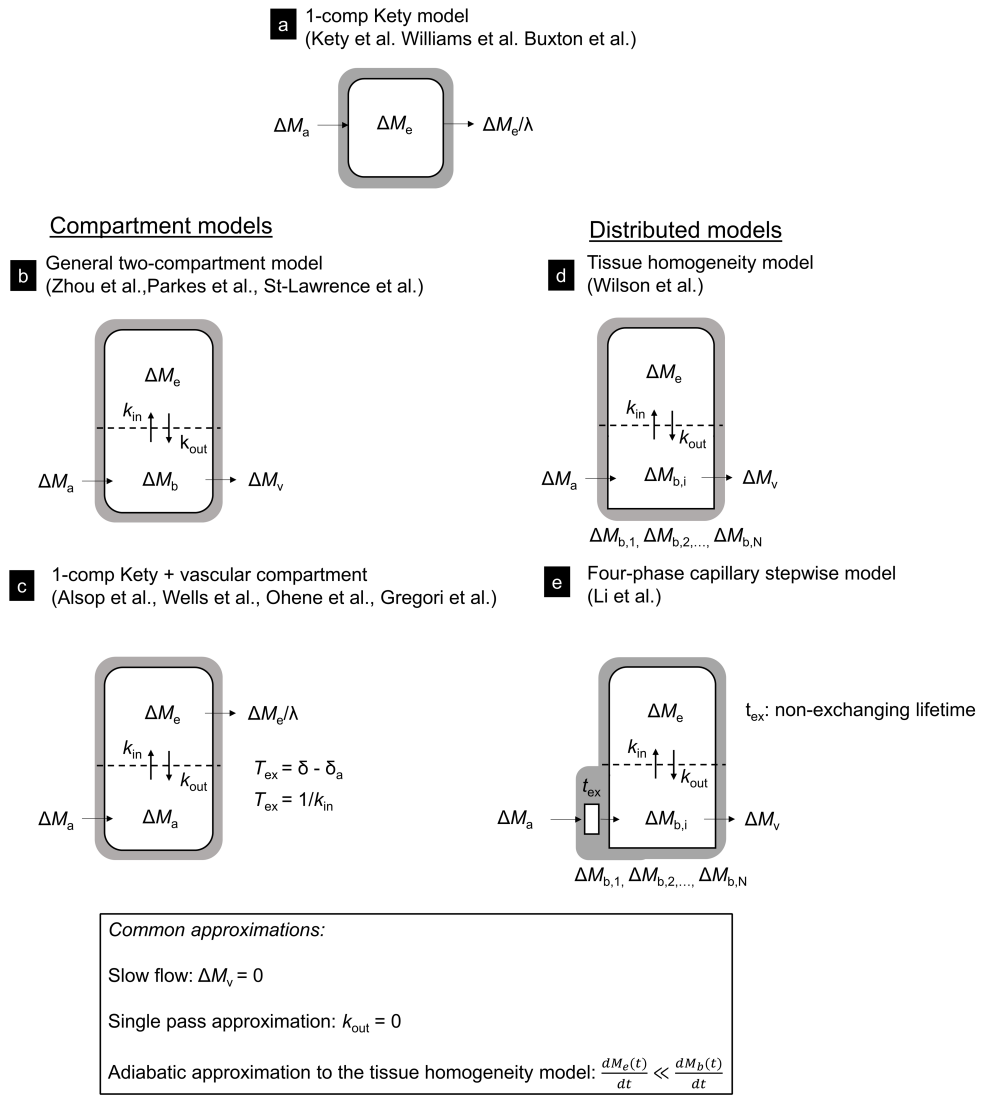

528

529 **Figure 4.** Kinetic models for measurement of BBB water exchange using ASL. **a** the standard Kety
530 model used for most ASL CBF measurements. The lack of a vascular compartment leads to bias in
531 CBF estimates when blood-tissue T_1 differences are large (i.e., in white matter), and when venous
532 water has not equilibrated fully with tissue water (i.e., high flow). **b** The general two-compartment
533 exchange model. Common approximations to this model include the slow flow approximation, which
534 assumes that $\Delta M_v = 0$, and the single pass approximation (SPA) which assumes that label does not
535 have time to re-exchange back into the blood compartment before the measurement time. **c** The Kety
536 model with an 'adhoc' vascular compartment. In contrast to the general two-compartment model, the
537 input to the extravascular compartment is the same as the input to the vascular compartment (i.e.,
538 $\Delta M_b = \Delta M_a$). **d** The general tissue homogeneity model, in which the vascular space is modelled as a
539 plug flow instead of a well-mixed compartment (distributed compartments designed by square edges).
540 Common approximations with time domain solutions include the SPA and adiabatic approximation
541 (AATH).**e** The four phase capillary stepwise model of Li et al. A non-exchanging compartment is
542 included to account for transit through larger non-exchanging vessels.

543

544

6.1 Contrast agent based approaches

Contrast agent based approaches aim to modify the T_1 of blood water using an exogenous intravascular contrast agent, such that the combined relaxation of the voxel (intra- and extravascular spaces) relaxes in a manner dependent on the BBB water exchange. If the sum, $k_{in} + k_{out}$, is much greater than the magnitude difference in intra- and extravascular relaxation rates, then water will be able to sample both compartments before substantial relaxation can occur, leading to mono-exponential 'exchange rate independent' T_1 relaxation. This condition is met under most 'non-contrast' conditions in both gray and white matter. For example, in gray matter, the difference in relaxation rates between intra- and extravascular spaces is of the order $\Delta R_1 = |1/T_{1e} - 1/T_{1b}| \sim |1/1.5 - 1/1.7|\ s^{-1} \sim 0.078\ s^{-1}$ at 3T [52,53] , which is much smaller than the sum of typical BBB water exchange rates, $k_{in} + k_{out} \sim 3\ s^{-1}$ [28]. In white matter, the blood and tissue T_1 values are more different, yet ΔR_1 remains much smaller than $k_{in} + k_{out}$, for example $\Delta R_1 \sim |1/1.1 - 1/1.7|\ s^{-1} \sim 0.32\ s^{-1}$ [52].

In the presence of an intravascular contrast agent, blood water T_1 becomes shorter and intravascular-extravascular relaxation rate differences become of the order of $k_{in} + k_{out}$ or larger. For example, assuming a blood contrast agent concentration of 1 mM (a typical post contrast concentration during the washout period following a standard dose of gadolinium contrast media in humans [54]) and contrast agent T_1 relaxivity $r_1 \sim 4.5\ (s\ mM)^{-1}$, intravascular-extravascular relaxation rate differences in gray matter are of the order $\Delta R_1 \sim |1/1.5 - 1/0.20| \sim 4.3\ s^{-1}$, which is greater than $k_{in} + k_{out}$. Under these conditions ($\Delta R_1 > k_{in} + k_{out}$), the system is in the intermediate/slow exchange regime, and the observed T_1 relaxation of the voxel is bi-exponential and exchange-rate dependent. By acquiring MRI images in both fast, and intermediate/slow exchange regimes, exchange rate information can be distinguished from other factors affecting MRI signals, including intrinsic relaxation rates, and water population fractions. The following sections describe approaches that utilize contrast agents to modify blood T_1 in order to measure water exchange across the BBB.

6.1.1 Dose ramping at steady state with a varied infusion rate

572 Schwarzbauer et al. measured BBB PS_w in rats at 7T using a stepped infusion technique
573 [26]. As the infusion rate was increased, T_1 values of tissue and blood were measured in a
574 single slice using a snapshot inversion-prepared spoiled gradient-recalled echo sequence
575 (IR-SPGR). Each time the infusion rate was increases, relaxation of blood and extravascular
576 water was pushed further towards the intermediate-slow exchange regime, resulting in a
577 series of tissue T_1 measurements with varied sensitivity to BBB water exchange. To maintain
578 constant blood concentrations for the duration of each T_1 measurement, a macromolecular
579 contrast agent expected to have minimal BBB leakage and renal excretion was used (Gd-
580 DTPA-polylysine, 75 kDa). The range of ΔR_1 values obtained was ~ 0.05 – 12 s^{-1} (as read
581 from Figure 5 in [26]).

582 A simplified two-compartment exchange model was used to describe the dependence of
583 tissue T_1 on p_b and PS_w (Equations 10-11 with $a_S = 0$). Measurements of PS_w were made by
584 fitting Eqn 15 ($T_{1,L}$ solution) to measured tissue T_1, essentially assuming the vascular
585 contribution to measured signals can be ignored. The validity of this assumption was tested
586 by taking the ratio of vascular to extravascular contributions to simple bi-exponential
587 relaxation, and found to be less than 3%, even at the highest contrast agent concentration.
588 However, the authors' analysis neglected the effects of the SPGR readout on evolution of
589 magnetisation, and errors may be larger than stated.

590 Rooney et al. applied a similar approach to measure BBB PS_w in subjects with glioblastoma
591 multiforme [28]. Instead of infusing the contrast agent, 3 injections of the superparamagentic
592 iron oxide nanoparticle (SPION) ferumoxytol were used to modify blood T_1. The use of
593 SPIONs in these cases was crucial to avoid any tissue T_1 effects caused by leakage of the
594 contrast across the BBB. p_b and k_{in} were measured in a single slice using a similar IR-SPGR
595 sequence, model and assumptions to those of Schwarzbauer et al. By using fewer injections
596 and T_1 measurements, the total measurement duration was reduced to 40 minutes
597 compared to 2 hours for the Schwarzbauer et al. protocol. The range of blood-tissue R_1
598 differences were of a similar magnitude (ΔR_1 ~ 0.04 – 14 s^{-1} (as read from Figure 5 in [28]).

599 Unfortunately, SPIONs are not widely approved use as diagnostic agents in humans, and
600 many candidate SPIONs have failed to gain regulatory approval, or have been withdrawn
601 from the market [55]. Intravascular gadolinium-based agents, such as gadofosvoset, may be
602 more translatable.

603 *6.1.2 First pass methods*

604 First pass methods for measuring BBB water exchange were first proposed by Anderson et
605 al. with a focus on detecting subtle BBB abnormalities in Alzheimer's disease [27] and then
606 developed further by the same laboratory in 2015 [28]. The method uses a dynamic contrast
607 enhanced MRI acquisition to rapidly acquire T_1 weighted images before and after a bolus
608 injection of an intravascular T_1-shortening contrast agent. Both studies used gadoteriodol as
609 contrast agent. By measuring T_1 prior to the injection of the contrast agent, T_1 weighted
610 signals acquired during bolus passage were converted into quantitative T_1 values.

611 Because the method is applied as the contrast agent passes through the tissue for the first
612 time, the arterial blood contrast agent concentration has the potential to reach ~ 5-10 mM in
613 approximately 10-20 seconds, depending on injection speed, contrast agent dose, and
614 cerebral perfusion. The main advantage of this approach is therefore being able to sample a
615 wide range of water exchange conditions in a very short timeframe. In this study, the range
616 of blood and tissue ΔR_1 values obtained during first pass was lower than in the dose
617 ramping studies discussed above (ΔR_1 = 0.05 – 2.6 s^{-1}, as read from Figure 1 in [28]), but
618 the effect was sufficient to enable robust voxelwise estimation of p_b and k_{in}. A relatively low
619 dose of gadoteriodol was injected relative to the typical doses given for low molecular weight
620 agents (28 μmol/kg versus 100 μmol/kg). Much larger effects, and more precise estimates
621 could be obtained by injecting larger doses. For example, in the case of intact BBB, a
622 standard dose of low molecular weight contrast media could be expected to produce
623 changes in ΔR_1 of between 0.05 – 23 s^{-1}, based on a T_1 relaxivity of 4.5 (mM s)-1 and
624 assuming a peak contrast agent concentration of 5 mM.

However, because of the rapidly changing contrast agent concentrations, temporal resolutions of approximately 1-2 seconds were required to capture the required information, limiting coverage to a single slice. Modern acceleration methods such as compressed sensing and multi-banding may enable full brain coverage, or an even higher sampling rate during the bolus passage. Delay and dispersion of the bolus as it passes through the capillary bed also means that capillary contrast agent concentrations are unlikely to be equal to those at the arterial or venous measurement points, which may lead to errors in estimates of k_{in} and PS_w.

6.1.3 Water exchange index (WEI) method

A number of studies have shown that BBB water exchange causes bias in steady-state cerebral blood volume estimates made using pre- and post-contrast spoiled gradient echo acquisitions [56–58]. In an attempt to minimize these biases, investigators have typically used flip angles and repetition times that minimise the effect of water exchange on MRI signals [56,59]. Based on this concept, Kim et al. develop a measure of BBB water exchange based on quantifying the degree of bias in cerebral blood volume estimates obtained when using flip angles that are sensitive to BBB water exchange, relative to flip angles that are insensitive to water exchange [29,58]. This approach produces a water exchange index (WEI) that is approximately linearly dependent on the water exchange rate (k_{in}), and only minimally dependent on CBV. Advantages include simple acquisition approach, full volume coverage, and no requirement for complicated modelling. Limitations include a strong dependence of WEI on TR, meaning that sequence standardization is required to ensure WEI values can be compared across studies. The approach also requires an intravascular contrast agent with a long circulating half-life such that the concentration of the agent in blood is the same for all post contrast images. Despite these limitations, this approach has undergone the most validation. Several studies have shown alterations in WEI in acute stroke models [29,60] and further studies have demonstrated its sensitivity to BBB changes caused by hypertonic mannitol and CO_2 challenge in the mouse brain [30].

6.1.4 Multiple flip angle multi-echo (MFAME)-MRI

MFAME-MRI, proposed by the authors' group, adapts the approach of Kim et al. to obtain quantitative estimates of PS_w with full brain coverage [31]. The approach makes use of clinically approved low molecular weight contrast agents, e.g. gadolinium-DTPA, or gadolinium-DOTA, with the *a priori* assumption that it remains intravascular, or that the leakage rate is low ($K^{trans} < 10^{-3}$ min^{-1}).

T_1-weighted images are acquired as in a standard dynamic contrast enhanced MRI acquisition. However, instead of maintaining a constant flip angle throughout, the post contrast flip angle is varied, providing images with a range of τ_b and p_b sensitivity. A long TR is used to enable multiple gradient echoes to be acquired per TR for T_2* decay correction. A general two-site water exchange model (Eqns 10-11) is then fit to the decay-corrected multi-flip angle signals to determine PS_w. Because the full 2-site exchange model is fitted, rather than the simplified two-site model applied by Schwarzbauer et al. and Rooney et al, possible errors caused by disregarding the vascular contribution are removed.

Due to the dependence of this approach on signals acquired at a range of different flip angles, accurate measurement of PS_w relies on homogeneous RF transmission (e.g., adiabatic excitation), or accurate measurement of a B_1 map. In addition, the two-site water exchange model becomes inaccurate if significant leakage of contrast agent occurs. It was shown that for low leakage rates, τ_b and p_b are overestimated, but because PS_w is the ratio of these two parameters, it is mostly unaffected. At larger leakage rates, estimates of PS_w are likely to be biased, unless accumulation of contrast agent in the extravascular space via BBB leakage is explicitly accounted for. This may, in principle, be achieved from the same set of measurements, although practical implementation is an area of active research.

6.2 Approaches based on arterial spin labelling (ASL)

While models accounting for water exchange have been shown to improve accuracy of CBF measurements [38,51], individual estimates of water exchange rates derived from standard

ASL data are imprecise [38,41]. This is due to the relatively small difference in blood and tissue T_1 relaxation rates relative to the exchange rate, making it difficult to detect the separate contributions of intravascular and extravascular label to the total ASL signal.

The following subsections describe a number of proposed methods that aim to improve the ability to distinguish the proportions of labelled water in blood and tissue.

6.2.1 Multi-TE ASL

In 2009, Wells et al. showed that the multi-compartmental origin of labelled water could be determined using multi-echo ASL at 9.4 T [61]. The apparent T_2 of labelled water was found to increase with increasing post-labelling delay time, reflecting passage of water from a short T_2 compartment (blood) to higher T_2 compartment (tissue). Following on from this study, Wells et al. applied the same approach to quantify the BBB pre-exchange water lifetime (T_{ex}, where $T_{ex} = \tau_b$) in mouse cortex, also at 9.4T [47]. Multi-echo subtraction signals were fitted with a bi-exponential T_2 decay model to extract intravascular and extravascular fractions as a function of post-labelling delay (PLD) time:

$$\Delta M(PLD, TE) = \Delta M_b(PLD) e^{\frac{-TE}{T_{2,b}}} + \Delta M_e(PLD) e^{-\frac{-TE}{T_{2,e}}} \qquad (21)$$

To constrain fits, T_2 of the extravascular space (long T_2) was estimated first by fitting a mono-exponential model to the control data (unlabelled data), then fixed in the bi-exponential fit of Eqn 21 (with $T_{2,control} = T_{2,e}$) to the subtraction data. Estimates of ΔM_b and ΔM_e were then input into the adapted Kety model (Figure 4c) to estimate the pre-exchange water lifetime. The mean cortical pre-exchange lifetime (± s.e.m) averaged across mice was 370 ± 42 ms. Reliable estimation of pre-exchange lifetime in brain regions other than the cortex were not possible (e.g. hippocampus and striatum) due to poor precision of the bi-exponential fits, highlighting the challenge of achieving adequate signal to noise ratio using this approach.

Gregori et al. applied a similar approach to estimate BBB water exchange in the human brain [48]. A more complete model that jointly accounted for T_1 and T_2 decay was fitted, assuming negligible backflow of label from tissue to blood and no venous outflow. This model was based on the general kinetic model of Buxton et al. for pulsed ASL acquisitions, yielding estimates of T_{ex} of 440 ms.

In all these approaches, the pre-exchange lifetime T_{ex} is calculated by subtracting the arterial transit time measured in a separate acquisition from the total tissue transit time (time from labelling to exchange) as modelled by the adapted Kety model ($T_{ex} = \delta - \delta_a$). The method therefore relies on reliable estimation of arterial transit times, which may be problematic in mice due to very high blood velocity. Optimised methods for measuring arterial transit times in rodents should be used if possible [62]

The ability to quantify water exchange using multi-TE ASL depends entirely on intrinsic R_2 differences between intravascular and extravascular water (Table 2). As field strength increases, the R_2 values of both blood and extravascular water increase; however, blood R_2 increases faster than extravascular R_2. Published data suggest that at 1.5T, R_2 of blood water is lower than R_2 of extravascular water; however this relationship is reversed at or above 3T for partially deoxygenated blood (80% oxygenated) and at or above 9.4T for 100% oxygenated blood [47,52,63–67]. Differences between blood (80% oxygenation) and tissue R_2 are similar for field strengths between 1.5T and 7T, (approximately 3-6 s^{-1}), but increase rapidly to approximately 40 s^{-1} at 9.4T due to the much higher R_2 of blood water.

Table 2. Blood and tissue R_2 variations with field strength. Blood R_2 values were taken from data with hematocrit in the range 0.4-0.45. References: a. Wansapura et al. [63], b. Stanisz et al. [52] c. Cox et al. [64], d. Krishnamurthy et al. [65], e. Zhao et al. [66], f. Silvennoinen et al. [67], g. Wells et al. [68]

Field strength	R_{2b} (s^{-1};100% O_2)	R_{2b} (s^{-1},80% O_2)	R_{2e} (s^{-1}, gray matter)	R_{2e} (s^{-1}, white matter)
1.5T	6.5[f]	7.0[f]	10.5[b], 11.9[c]	13.9[b], 10.6[c]
3T	8.8[e]	18.3[e]	12.5[a], 10.1[b,] 15.9[c]	9.1[a], 14.5[b,] 13[c]
7T	16.7[c]	25[c]	25.6[c]	20[c]
9.4T	30[g]	66[g]	26.3[g]	-

The strong dependence of R_2 on blood oxygenation level is likely to alter the precision of T_2-based water exchange measurements in an oxygenation-dependent manner (Table 2). At 9.4T, Wells et al. report that as the oxygenation of blood increases to near 100%, precision in estimates of T_{ex} is 'markedly lower than under air', because of the similarity of $T_{2,b}$ and $T_{2,e}$ values under these conditions. Table 2 shows that at 7T, the opposite effect is expected, with greater R_2 differences at 100% oxygenation than at 80% oxygenation. For preclinical studies using T_2 to quantify BBB water exchange, the choice of anaesthetic carrier gas should be carefully considered.

6.2.2 Diffusion-weighted ASL

The pseudo-diffusion coefficient of vascular spins due to perfusion is approximately 10 times that of extravascular spins [69]. By applying diffusion sensitising gradients of low strength, vascular spins can be nulled, leaving only signal from spins in the extravascular compartment. Therefore, by applying diffusion weighting following labelling in ASL experiments, the proportion of label in each compartment can be determined as a function of post labelling delay time.

Silva et al. first applied diffusion weighting to separate vascular and extravascular contributions to ASL signal in rats [70]. Diffusion gradients were applied at 12 b-values along a single direction immediately after a 3.5 s labelling pulse. Through applying an intra-voxel

incoherent motion (IVIM) type model to the subtraction images, the authors were able to estimate the fast (intravascular) and slow (tissue) diffusing fractions of the label and their respective pseudo-diffusion /diffusion coefficients:

$$\frac{\Delta M(t,b)}{\Delta M(t,b=0)} = A_1(t)e^{-bD^*} + A_2(t)e^{-bD} \qquad (22)$$

where t is the PLD time and $A_1(t) + A_2(t) = 1$. The amplitude of the extravascular fraction was found to decrease with hypercapnia, corroborating the expected decrease in the extraction fraction with increasing CO_2 tension.

This basic approach was developed further by Wang et al. [71] by explicitly expressing the amplitudes of diffusion components A_1 and A_2 in terms of intravascular and extravascular label fractions:

$$A_1(t) = \frac{\Delta M_b(t)}{\Delta M(t)} \qquad (23)$$

$$A_2(t) = \frac{\Delta M_e(t)}{\Delta M(t)} \qquad (24)$$

This description enabled measurements of A_1 and A_2 to be input into exchange models to estimate k_{in}. By assuming values for the arterial transit time, T_1, and T_2, and by measuring the amplitudes A_1 and A_2 using multiple b value (7 b-values, 0 – 300 s mm^{-2}) single delay time (PLD = 1.2 s) ASL, Wang et al. were able to estimate k_{in} using the SPA model. The PLD time was assumed to be longer than the arterial transit time, but shorter than the tissue transit time. In other words, it was assumed that the label was exchanging across the BBB at the measurement time.

Additional measurements of A_1, A_2, D and D^* were made for a number of PLDs to demonstrate the signal behaviour as a function of delay time. The authors observed that as the delay time increased from 800-1500 ms, the fraction of fast-diffusing label (assumed to be intravascular) diminished from approximately 39% to 15%, consistent with exchange of label across the BBB. The diffusion coefficient of the fast diffusing compartment (D^*)

765 decreased from 0.34 $mm^2 s^{-1}$ at PLD = 800 ms to 0.069 $mm^2 s^{-1}$ at PLD = 1500 ms, indicating
766 the presence of multiple flow regimes.

767 To speed up the data acquisition, the authors also presented a simplified method for
768 estimating k_{in} using only two b-values (0 and 50 s mm^{-2}), and applied this approach to a
769 brain tumour patient (grade II, oligodendroglioma). They showed that a b-value of 50 s mm^{-2}
770 spoils nearly all intravascular magnetisation (>98%) but very little extravascular
771 magnetisation (< 5%). Assuming that a bipolar gradient with b = 50 s mm^{-2} spoils all the
772 intravascular magnetisation, the amplitudes can be approximated using the following
773 expressions:

774 $$A_2(t) \cong \frac{\Delta M(t, b = 50)}{\Delta M(t, b = 0)}$$

775 $$A_1(t) \cong 1 - \frac{\Delta M(t, b = 50)}{\Delta M(t, b = 0)}$$

776 This two-point approach elegantly removes the need to model intravascular flow
777 characteristics, which can vary as the label moves from arteriole to capillary (see above).
778 Since blood in arterioles has a velocity greater than in capillaries, all downstream label will
779 be nulled regardless of its pseudo-diffusion coefficient. The approach will fail to produce
780 accurate estimates if the PLD is shorter than the arterial transit time (k_{in} overestimated), or if
781 exchange has completed by the time of measurement (combination of short arterial transit
782 time and high k_{in}). Longer delay times will likely be beneficial for ensuring label is most
783 consistently within the capillary compartment across subjects, but this must be balanced
784 against the loss of label due to T_1 relaxation.

785 Since labelling occurs non-locally to the voxel of interest, estimation of k_{in} requires
786 knowledge of the arterial transit time. The same is true for all ASL based measurements of
787 BBB water exchange. St. Lawrence et al. proposed estimating arterial transit time using a
788 DW-ASL acquisition with b value of 10 s mm^{-2} at an intermediate PLD [72,73]. The b-value
789 of 10 s mm^{-2} was chosen to crush label in the arterial compartment, while leaving capillary

and tissue label unaffected. By comparing images with and without arterial crushers it is possible to deduce when the label arrives at the tissue, if CBF is known or can be estimated. The post-labelling delay time is set to be long enough such that the labelled blood has arrived in the imaging slice, but short enough such that exchange has not occurred (i.e. the label remains primarily in the arterial compartment).

Recently, Wengler et al. proposed a method for measuring BBB water permeability based on the intrinsic diffusion sensitivity of segmented gradient and spin echo (GRASE) readouts [74]. In the image domain, pseudo-diffusion due to perfusion manifests as a point spread function (PSF) that causes significant image blur. Meanwhile, the extravascular compartment experiences only negligible diffusion sensitivity along the echo train, resulting in different PSFs for the intravascular and extravascular spins. The difference image between label and control is given by:

$$\Delta M = A_1 \cdot \Delta M_{true} * PSF_b + A_2 M_{true} * PSF_e$$

where ΔM_{true} is the true difference image in the absence of point spread function effects, A_1 and A_2 are the relative amplitudes of the label in intravascular and extravascular spaces repsecitively, and PSF_b and PSF_e are the point spread functions of intravascular and extravascular label contributions due to pseudo-diffusion and diffusion respectively. The $*$ operator denotes convolution. Data with different segmentation schemes were acquired at a PLD = 2000 ms, varying the blurring effects of the vascular spins. The effect of the PSFs on the measured signal was estimated using augmented extended phase graphs, yielding estimates of A_1 and A_2, which were then input into a version of Alsop's two-compartment model [46], adapted to account for extraction fractions less than 1. The authors assume that exchange has completed by the time of imaging (PLD > $\delta_a + \tau_b$), and estimate *E* and *f* assuming that the exchange rate k_{in} is known and fixed. The Renkin-Crone equation (Eqn 1) is then used to estimate PS_w from *E* and *f*. The former assumption may not be valid in cases of high perfusion (i.e. in rodents). The latter assumption is odd since it imposes an unnecessary restriction that changes in *E* are due to changes in vascular transit time, not

changes in vessel permeability, P. Since vascular transit times are not measured, their method can at best estimate k_{in}, not PS_w as reported in the paper.

6.2.3. Magnetisation transfer weighted ASL

Silva et al. [75] proposed that intravascular and extravascular signals can be separated by their different magnetisation transfer effects. ASL pairs were obtained with and without saturation of macromolecules, and a two-compartment model used to describe exchange between brain water and macromolecular spins. By knowing that macromolecular spins interact more strongly with extravascular water, it was possible to deduce which compartment the label was in at any given post-labelling delay time. Steady-state (i.e. continuous labelling) measurements were obtained, and extraction fraction estimated.

6.2.4 Contrast-enhanced ASL

Estimating BBB water exchange from standard ASL data is challenging due to the similarity of blood and tissue T_1 values. In essence it becomes impossible to know in which compartment the label resides at the chosen delay time. The sections above describe methods to distinguish label compartments using T_2-weighting, diffusion-weighting, or MT-weighting. Another approach is to increase blood-tissue T_1 and/or T_2* differences using intravascular contrast agents.

Zaharchuk et al. proposed the continuous assessment of perfusion by tagging including volume and water extraction (CAPTIVE) method in 1998 [76]. The method focused on altering blood-tissue T_2* differences, while minimizing effects on T_1. This was done because a shorter blood T_1, usually the result of most paramagnetic contrast agents, would also reduce the amount of label reaching the tissue, thus significantly reducing the SNR of post-contrast images. To minimize T_1-shortening effects, a ‘shift reagent’ long circulating agent (MPEGs-PL-DTPA) was used, which had a large effect on blood and tissue T_2*, but only a small effect on blood T_1 and no effect on tissue T_1. This meant that label underwent similar T_1 relaxation in both pre- and post-contrast datasets, but that T_2* of blood and tissue was

much shorter post-contrast. Crucially, label residing in the intravascular space was assumed to be completely nulled in post-contrast images, leaving only label in tissue, albeit reduced significantly due to T_2* effects. Assuming T_1 effects were small, the ratios of pre- and post-contrast subtraction images acquired at long pulse labelling delay times were equated to the extraction fraction of labelled water. This approach is similar in concept to the DW-ASL measurement proposed by Wang et al. [71], where a low b-value is used to null intravascular label. The use of a contrast agent makes this approach more invasive, and is likely to have a lower SNR since the contrast agent reduces T_2* of tissue as well as that of blood.

A similar approach was proposed by the authors' group [77], but with several differences: i) a clinical T_1 shortening contrast agent was used (1/4 dose), demonstrating that label is still detectable, and highlighting the possibility for translation into humans, ii) multiple delay times were used, enabling arterial transit time to be estimated simultaneously with the BBB water exchange rate. T_2* effects were smaller due to the use of a contrast agent with lower r_2* relaxivity. The data suggested that a two-compartment model provided a substantially better fit across all delay times than a purely vascular or purely extravascular model. Sensitivity to water exchange increased as contrast agent dose increased from 0.8 mL to 2.1 mL of Gd-DOTA, with estimates of PS_w decreasing from 67 mL min^{-1} mL^{-1} to 1.5 mL min^{-1} mL^{-1} as contrast agent dose was increased.

6.2.5 Phase-contrast ASL

The water-extraction-with-phase-contrast-arterial-spin-tagging (WEPCAST) method takes a unique approach to measuring PS_w by quantifying the transmitted fraction of labelled water passing into the superior sagittal sinus (SSS) during a single pass [78]. Models often assume label reaching the venous compartment is small or negligible due to T_1 relaxation. In this study, the authors show that when using multiple long delay times and pCASL, it is possible to detect labelled water in the SSS, provided sufficient background suppression is applied.

Simulations performed in the study showed that the non-extracted fraction contributed approximately 84% of the SSS signal, relative to label that re-exchanged back into the bloodstream following leakage across the BBB. The SSS signal from subtraction images was shown to increase with PLD time, reaching a maximum of 0.3-0.6% at approximately 2.5-3.5 s, then decreasing to approximately 0.1-0.2% at 4.5 s. The authors show a spatially dependent signal enhancement throughout the SSS, reaching peak enhancement first in the anterior SSS (at delay time of 2.5 s), and last in the posterior SSS (at a delay time of 3.5 s). The authors then attempt to improve the detection sensitivity by including bi-polar phase-contrast velocity-encoding gradients to better isolate signal arising from voxels containing pure blood (i.e. the SSS), and remove that from voxels containing both blood and tissue (i.e. voxels close to the SSS that would interfere via partial volume effects). In these datasets, a quantitative model describing label contributions in the SSS is fitted to subtraction images to estimate the global cerebral blood flow, and extraction fraction, from which whole-brain PS_w is estimated using the Renkin-Crone model.

Like the two-compartment ASL models applied to DW-ASL, the WEPCAST model requires knowledge of blood and tissue T_1, which are fixed to literature values (but could in principle be measured). Furthermore, the model accounts for temporal smoothing of the label as it passes from the artery to SSS, likely improving model accuracy but adding additional parameters to estimate alongside E and cerebral blood flow. Unfortunately, because the method relies on measuring label in a large draining vein, it can only estimate global BBB permeability, with no regional information. Combining WEPCAST with vessel-encoding arterial tagging [79] may enable regional information on BBB permeability to be determined.

6.3 Approaches based on injection of MRI-detectable water tracers

Approaches described so far measure the trans-BBB exchange of endogenous water. Another class of methods, similar in design to ^{15}O-labelled water PET, aims to detect trans-BBB exchange of injected water, enriched with either ^{2}H (deuterium) [80–82] or ^{17}O [83–91]. Such isotopes can be detected directly using multinuclear probes [80] or indirectly via their

effect on ^{1}H relaxation [87] or, in the case of deuterium, effects on proton density. This review will not discuss direct measurement and focusses mainly on indirect measurement techniques, due to their greater translational potential.

6.3.1 Indirect detection of ^{17}O-labeled water via its effect on ^{1}H T_2

^{17}O-labelled water alters the T_2 of ^{1}H protons via scalar coupling of ^{17}O–^{1}H. Detection of ^{17}O-labelled water using spin-echo based echo planar imaging (EPI) [90], T_2-weighted rapid imaging with refocussed echo imaging (RARE) [84,85,91], and steady state free precession sequences [86,92] have been proposed, enabling uptake and washout of ^{17}O-labelled water from the brain to be tracked with high temporal resolution (< 10 s). Ronen et al. proposed a simplified 2-point method by acquiring post-injection spin-echo images with and without sensitization to ^{17}O–^{1}H scalar-coupling [87]. This was achieved by collecting image sets with and without RF irradiation applied during the readout.

Two studies performed quantitative analyses of ^{17}O-labelled water enhancement curves. Igarashi et al. [84] and Huber et al. [85] observed very rapid uptake of labelled water into tissue and CSF spaces, followed by an equilibration phase that plateaued 300 s after injection. To describe the curve shape of the equilibration phase, the investigators fitted an empirical exponential decay model, $I = I_0 + a*\exp(-b*t)$ [84,85,91], with I_0 describing the steady state attenuation, and a the peak attenuation, and b the washout rate. Unfortunately, it was not clear from this study to what degree these parameters reflect BBB water exchange. In a similar study, Kudo et al. [86] estimated ^{17}O-labelled water concentration in tissue and cerebrospinal fluid by comparing signals to calibration phantoms, providing the possibility for quantitative kinetic analyses, and estimation of k_{in} or PS_w. These approaches provide dynamic kinetic information at high temporal resolution and SNR. The main disadvantage of the approach is the high cost of ^{17}O-labelled water.

6.3.2 Indirect detection of ^{2}H-labeled water by proton replacement

Early attempts to detect ^{2}H-labelled water were mainly by direct detection using ^{2}H receiver coils [80,82]. Indirect detection methods were not pursued until recently [81], possibly because of early evidence suggesting deuterium does not produce large effects on T_1 [93]. Wang et al. [81] presented a novel approach whereby ^{2}H-labelled water was detected by its proton replacement effect using EPI and RARE sequences. Since protons in ^{2}H-labelled water are invisible to ^{1}H MRI, as it perfuses and exchanges with tissue, the detectable ^{1}H signal reduces. Interestingly, ^{2}H-labelled water was also found to have negative relaxivity, increasing T_1 and T_2 of ^{1}H as its concentration increased. While potentially extremely useful to study BBB dysfunction in rodents, this approach may not translate well to humans as deuterium is toxic in large doses.

7. Summary of published results

7.1 Water exchange across the BBB in healthy brain tissue

Measurements of BBB water exchange in healthy brain tissue are summarized in Tables 3 and 4. Table 3 presents the actual measurements, and where missing, estimated values of k_{in} or PS_w assuming literature values for v_b. Table 4 presents the mean and standard error on the mean for k_{in} and PS_w in healthy human gray and white matter, and rodent gray matter averaged across studies presented in Table 3. T-tests were performed to test the null hypotheses of no difference in human gray and white matter water exchange parameters (using measurements from studies where both gray and white matter water exchange were measured in the same individuals), and no difference between human and rodent gray matter water exchange parameters. k_{in} was found not to differ significantly between healthy human gray and white matter ($p = 0.55$, paired t-test), whereas PS_w was significantly lower in white matter ($p = 0.0062$, paired t-test), primarily because of the lower blood volume. k_{in} and PS_w did not vary between human and rodent gray matter ($p = 0.62$ and $p = 0.98$ respectively, unpaired t-tests).

7.2 Water exchange across the BBB in disease

947 Trans-BBB water exchange has been evaluated across a range of diseases including stroke,
948 obstructive sleep apnea (OSA), Alzheimer's disease (AD), small vessel disease, multiple
949 sclerosis (MS) and tumours. Results are summarised in Table 5 and discussed in detail in
950 the following sections.

951 *7.2.1 Water exchange across the BBB in stroke*

952 Kim et al. measured the water exchange index (WEI) to quantify changes in BBB water
953 exchange in the acute stages following permanent middle cerebral artery occlusion (MCAo)
954 in mice [29]. In the ipsilesional cortex, WEI was increased relative to contralateral brain
955 tissue, indicating increased BBB permeability to water. Huang et al. evaluated WEI 1 hour
956 following ischemic stroke and reperfusion [60]. WEI was found to be elevated in the
957 ipsilateral cortex, and more severely altered in animals with lower ipsilateral CBV. The
958 authors posited that the increase in WEI in animals with poor reperfusion (i.e. as quantified
959 by CBV) reflected higher levels of BBB damage and increased water permeability.

960 Tiwari et al. used DW-ASL to measure water exchange in a mouse model of transient MCAo
961 90 minutes post stroke, then at 2 days post reperfusion [94]. At 90 minutes post occlusion,
962 no changes in k_{in} or the fraction of vascular label fraction were observed. Following
963 reperfusion, significant reductions in k_{in} and increases in the vascular label fraction were
964 observed. The authors suggest that changes in these parameters were caused by increased
965 BBB permeability to water; however, this interpretation is incorrect, as k_{in} is proportional to,
966 not inversely proportional to, BBB permeability. The authors show large increases in CBF in
967 lesioned tissue, possibly caused by a chronic vasodilatory response to hypoxia. Increases in
968 vessel radius resulting from this could reduce k_{in}, in the absence of any changes in vessel
969 permeability.

970 *7.2.2 Water exchange across the BBB in neurodegeneration*

971 The authors' group applied MFAME-MRI in a transgenic rat model of Alzheimer's disease
972 [31]. PS_w was found to be higher in AD rats relative to wild-types in several brain regions.

Using T_2-weighted imaging of ^{17}O-labelled water, Igarashi et al. found no difference in the steady-state level of $H_2{}^{17}O$ in a mouse model of AD [84], but CSF uptake was increased. Shao et al. used DW-ASL to measure k_{in} in patients at risk of small vessel disease [95]. k_{in} was found to be significantly higher in persons with diabetes and hypercholesteriemia. k_{in} correlated with white matter hyper-intensity severity, and was inversely correlated with episodic memory scores from a picture sequence memory test.

7.2.3 Water exchange across the BBB in obstructive sleep apnea

Palomares et al. assessed BBB water exchange rate in patients with OSA using DW-ASL [96]. Reductions in k_{in} were observed in OSA patients relative to controls. No changes in arterial transit time or cerebral blood flow were found. While no specific validation was performed, it was suggested that since OSA is accompanied by hypoxia and cerebral ischemia, reduced k_{in} could result from hypoxia-induced reductions in aquaporin-4 channels at the BBB.

7.2.4 Water exchange across the BBB in multiple sclerosis (MS)

Rooney et al. compared k_{in} between controls and subjects with relapsing remitting MS [28]. k_{in} was reduced in normal-appearing GM (k_{in} = 120 min^{-1} vs 174 min^{-1}), normal-appearing WM (k_{in} = 132 min^{-1} vs 186 min^{-1}), and lesion regions (k_{in} = 108 min^{-1}) relative to controls. In the same study, the authors hypothesized that changes to BBB k_{in} are driven by the metabolic activity of neurons via a chain of active transmembrane water cycling processes resulting from neuronal Na^+-K^+-ATPase activity. The contribution of ion pumps towards transcytolemmal water exchange is well established [97–99]; however the link between BBB water exchange and pump activity is not.

7.2.5 Water exchange across the BBB in brain tumours

Wang et al. found increased k_{in} compared to normal tissue in a single patient with grade II oligodendroglioma [71]. Conversely, Rooney et al. observed decreased k_{in} in 5 patients with glioblastoma multiforme [28]. These patients had prior surgical biopsy or resections followed

by chemo-radiation therapy. While decreased water k_{in} in these brain tumours is not implausible, it is counter-intuitive, since these tumours were also found to enhance on gadolinium-enhanced MRI, and yet the contrast agent is a much larger molecule than water. It was suggested that reduced k_{in} in these tumours was caused by reduced sodium pump activity; however no validatory evidence was provided to support this claim.

7.3. Water exchange across the BBB in knockout models

Using multi-*TE* ASL, Ohene et al. observed an increase in the pre-exchange lifetime of water in cortex of aquaporin-4 deficient mice (T_{ex} = 452 ± 90 ms) relative to wild-types (T_{ex} = 343 ± 91 ms), indicating a slower water exchange rate due to lower PS_w or higher p_b [100]. Measuring uptake of $H_2{}^{17}O$ tracer using T_2-weighted MRI, Igarashi et al. observed that the steady state level of $H_2{}^{17}O$ in the cortex of rats was unaffected by both aquaporin-4 and aquaporin-1 deletion [101].

Atochin et al. used the WEI approach to quantify trans-BBB water exchange in eNOS deficient mice [102]. eNOS is key signal transduction enzyme responsible for endothelium-dependent vasodilation, and cerebral blood flow. In knock-out mice, WEI significantly increased relative to wild-types.

7.4 Technical validation of BBB water exchange measurements in rodents

Several attempts to validate MRI-based BBB water exchange measurements have been made. Results are summarized in Table 6. The following section outlines the key results from these studies.

Hypertonic mannitol has been used to alter BBB physiology in a number of studies [30,75]. Mannitol does not cross the BBB, and produces an osmotic gradient between the blood and extravascular space, pulling water into the bloodstream, and shrinking endothelial cells. This increases cerebral blood volume, and widens inter-endothelial tight junctions to approximately 200 Å, increasing BBB permeability [103]. Silva et al. showed, using magnetisation-transfer ASL, that mannitol increased water extraction fraction, indicating

1025 increased PS_w [75]. Using the WEI method, Huang et al. observed increases in WEI and
1026 CBV as early as 15 minutes following mannitol injection [30].

1027 The effects of hypercapnia on BBB water exchange have also been studied. Hypercapnia
1028 causes vasodilation of capillaries and arterioles [104], increasing CBV and CBF. Increased
1029 leakage of injected tracers has been observed [105,106]; thus increases in water exchange
1030 would be expected either through an increased exchange area or increased number of open
1031 tight junctions. Using the WEI method, Huang et al. observed increases in WEI with pCO_2
1032 concentration [30]. Using DW-ASL, Silva et al. observed a reduction in the fraction of label
1033 remaining intravascular with hypercapnia, pointing towards increased k_{in} [70]. However,
1034 since hypercapnia reduces arterial transit time, the label will have had more time to
1035 exchange before it was measured. Zahaurchuk et al. measured PS_w with the CAPTIVE
1036 method, and found no change with increasing arterial pCO_2 concentration [76]. Overall, the
1037 effects of mannitol on BBB water permeability appear to be more robust than those of CO_2
1038 challenge.

1039 Others investigators compared water exchange measurements to established permeability
1040 assays such as dynamic contrast enhanced MRI and Evans blue staining. In a model of
1041 middle cerebral artery occlusion (MCAo), Tiwari et al. showed decreased k_{in} in the lesioned
1042 area following reperfusion [94]. The same animals were subject to dynamic contrast-
1043 enhanced MRI to measure the leakage rate of gadolinium-based contrast agent (K^{trans}) *in-*
1044 *vivo* and Evans blue perfusion to visualize BBB integrity *ex-vivo*. Both measurements
1045 confirmed the spatial distribution of DW-ASL changes, but showed increased leakage, not
1046 decreased leakage as predicted by their k_{in} measurements. These results support the
1047 potential for reduced BBB water permeability even in the presence of tight junction
1048 disruption, as reported by Rooney et al. in glioblastoma [28].

1049 The authors' group compared MFAME-MRI measurements of PS_w to the expression of BBB
1050 proteins occludin, claudin-5, and aquaporin-4 in the TgF344-AD rat model of AD, and also
1051 cross-validated against gadolinium-DOTA leakage, measured using dynamic contrast-

enhanced MRI [31]. Occludin was expressed less in AD rats relative to controls, and correlated inversely with PS_w. *G*adolinium leakage was not affected. This work indicates that measurements of water permeability are more sensitive to subtle tight junction changes of the type occurring in AD than measurements of gadolinium-DOTA leakage. .

Using an aquaporin-4 facilitator drug and T_2-weighted imaging of $H_2{}^{17}O$, Huber et al. showed steady-state signal loss (I_0) in the cortex was reduced relative to placebo, indicating an increased BBB turnover of $H_2{}^{17}O$ [85]. However, this measurement likely depends on CBF, as well as blood and extravascular volume fractions, which may have also changed.

7.5 Precision of water exchange measurements

The reliability and repeatability of water exchange measurements varies between methods, and depends fundamentally on the SNR of the data relative to the magnitude of water exchange effects. A precise BBB water exchange measurement should be capable of robustly separating intravascular and extravascular signal contributions in the presence of image noise. Factors including MRI coil sensitivity profile, readout bandwidth, voxel size, and the number of signal averages will also affect measurement precision.

Standard ASL provides low sensitivity to water exchange, with estimation of k_{in} often failing entirely in both gray and white matter. In 2007, Carr et al. noted that to measure PS_w with even a 100% coefficient of variation would require an SNR increase of approximately 2 orders of magnitude, based on a typical ASL acquisition of the time [41]. Rodent studies using multi-TE ASL [47,100] failed to provide reliable estimates outside the cortex, while the human multi-TE ASL produced reliable estimates only in gray matter regions [48]. Contrast agent based approaches were able to estimate k_{in} in multiple cortical and subcortical gray matter regions [26,31]. First pass contrast agent methods and diffusion-weighted ASL approaches are the only methods to date that have demonstrated sufficient SNR to enable reasonable voxel-wise estimates across gray and white matter in the human brain [28,72,95].

Several studies have formally measured scan-rescan reproducibility. Using DW-ASL with a 2D readout, St Lawrence et al. measured scan-rescan reproducibility (intra-subject coefficient of variation) of k_{in} to be 26% and 21% for gray and white matter regions respectively [72]. Using a DW-MRI with a 3D readout, Shao et al. obtained intra-subject correlation values of 0.52-0.72 in cortical regions, 0.30 in the hippocampus, 0.57-0.74 in the cingulum, and 0.63 in the precuneus [95]. Unpublished data from the author's group show that scan-rescan coefficient of variation for regional PS_w estimates obtained using MFAME-MRI is approximately 40%. No data currently exist on the scan-rescan reproducibility of first pass contrast-enhanced methods, or of multi-TE ASL.

8. Validity of a two-site model for BBB water exchange

Models used to estimate BBB water exchange typically assume that intravascular and extravascular compartments are well-mixed. This section discusses the validity of this assumption.

In the intravascular space, water exchange rates across the red-blood cell membrane (intracellular to plasma) are of the order of 50-100 s^{-1} [107]. Using Eqn 8, and assuming a haematocrit of 42%, the water exchange rate from plasma to the intracellular space is approximately 36-72 s^{-1}, giving an average exchange rate of 43-86 s^{-1}.

In the extravascular space, the water exchange rate from the intracellular to interstitial compartment is of the order 1.4-2 s^{-1} [108], depending on cell type. Assuming brain cells in gray matter (neurones and glia) occupy approximately 80% of the extravascular volume (assuming ~20% is taken up by interstitial volume [109]), the exchange rate from the interstitial compartment to the intracellular compartment is of the order of 5.6-8 s^{-1}. The average exchange rate across the cellular membrane is therefore approximately 4.2-5 s^{-1}.

This exchange rate is much lower than that across red-blood cells, primarily because of the larger size of brain cells.

The water exchange rate across the BBB from intra- to extravascular space (k_{in}) is approximately 2.5 s^{-1} (taken from Table 4, calculated by taking the mean value across human gray and white matter, and rodent brain = 151 min^{-1}). Assuming a blood volume of 5%, the exchange rate from the extravascular space to the intravascular space is approximately 0.16 s^{-1}, giving an average exchange rate across the BBB of 1.3 s^{-1}.

Water exchange across the BBB is therefore approximately 40 times slower than that across red-blood cells, and approximately 3.5 times slower than that across brain cell membranes. It appears therefore that a two-compartment model may be a good assumption. However, while faster than BBB exchange, exchange between intravascular and extravascular sub-compartments may still not be sufficient to average together their relaxation and diffusion properties. Experimental evidence suggests that bi-exponential T_2 relaxation [24,25,107] and diffusion occurs [110] in the intravascular space, and that extravascular diffusion is multi-compartmental [111]. Further work is needed to determine whether the limitations of water exchange across the BBB are sufficient to dominate relaxation or diffusion effects over those occurring within intra and extravascular compartments, or whether by ignoring these contributions, estimates of k_{in} and PS_w become biased.

9. Physiological specificity of BBB water exchange measurements

Contrast agent approaches provide greater physiological specificity than ASL-based approaches, as they are able to directly measure both k_{in} and PS_w. From a biological point of view, it is not yet clear which parameter is likely to be most sensitive to pathology. Both k_{in} and PS_w depend linearly on vessel permeability. They both also depend on vessel radius (R), but in different ways. k_{in} is inversely proportional to R, whereas the change in PS_w due to changes in R, depends on whether the vessel surface area remains constant (i.e.

increased vessel radius, but reduced vessel density) or changes (i.e. vasodilation at constant vessel density). The dependence of k_{in} and PS_w on vessel radius could be exploited to isolate P via combined measurement of BBB water exchange and vessel size.

10. Conclusions

Studies undertaken so far report a wide range of k_{in} and PS_w values. These values are higher than for radioisotope methods by a factor of approximately 3-6. The reasons for this bias are currently unclear and require further study, with the current generation of MR-PET hybrid scanners providing an excellent opportunity for real-time direct comparison. Some methods appear to have superior sensitivity, but scan-rescan reproducibility data for all methods is lacking, making a valid comparison difficult. In rodents, where high doses of contrast agents can be used, contrast agent based approaches provide robust estimates of regional BBB water exchange. The two-point DW-ASL method of Wang et al. [71] has been applied the most frequently in clinical studies, and appears to provide robust estimates of k_{in} in human gray and white matter, as well as being entirely non-invasive. All ASL-based measurements of BBB water exchange depend on being able to accurately estimate arterial transit time. Care should be taken as biases in arterial transit time will propagate through to create bias in k_{in}.

Literature summarised in this review shows BBB water exchange is altered in a wide range of diseases, including stroke, Alzheimer's disease, small vessel disease, diabetes, obstructive sleep apnea, multiple sclerosis, and cancer. In some applications, BBB water exchange rate increases (stroke, AD, smallvessel disease), indicating increased BBB permeability to water. In others (e.g. glioblastoma, obstructive sleep apnea), water exchange is reduced, indicating reduced water permeability, although apparently contradictory results cloud this picture. Further work is needed to understand the factors that contribute towards increased and decreased BBB water exchange in these conditions.

While a number of putative water transport routes are known, the physiological role of equilibrium BBB water exchange, and the contribution of each different transport pathway to normal and pathological brain functioning are poorly understood. This compares starkly with osmotically obliged water transport (non-equilibrium water exchange), which has been extensively studied due to its acute impact on health in stroke and traumatic brain injury [112]. There are currently many unresolved questions relating to equilibrium water exchange. Does equilibrium water exchange serve any physiological purpose (e.g. clearance of waste products, cell hydration), or is it a physical phenomenon with little biological impact? Does altered water transport indicate abnormalities in other potentially harmful processes (e.g. altered amyloid-β clearance)? What is the principal route through which water travels across the BBB? What effect does increased or decreased equilibrium water exchange have on brain function? To what degree do physical barriers such as pericytes, basement membranes, and astrocyte end-feet limit entry of water into the brain? Is there a preferential destination for water upon entry into the brain (i.e. path of least resistance)? Do passive and active water transport processes impact on or interact with one another? These questions should be investigated in future BBB water exchange studies.

While there are currently many excellent approaches for measuring water exchange using MRI, there are also many opportunities to further improve these measurements. Simultaneously measuring the effect of BBB water exchange on multiple MRI contrasts (e.g. T_1, T_2, D), and jointly modelling these effects may increase precision and accuracy over that achievable using existing measurements. For example, acquiring diffusion-weighted ASL at multiple echo times may help to better define label location, and therefore k_{in} [113]. Furthermore, simultaneously measuring the effect of exchange on T_1 and T_2 in contrast agent based methods (e.g. using a steady state free-precession sequence) may also help [114]. Since T_2 relaxation rates are inherently 1-2 orders of magnitude greater than T_1 relaxation rates, much faster water exchange is required to average compartmental relaxation rates, than for T_1. This means that very fast exchange rates, as may be present in

cases of severe BBB breakdown, and which would be difficult to measure precisely with T_1 contrast alone, may be more precisely measured via their effect on T_2.

In conclusion, MRI measurements of BBB water exchange have already contributed significantly to understanding of BBB dysfunction across a range of disease settings. Future work should aim to improve the repeatability of these measurements, such that they can be used to better understand the timing and origin of BBB dysfunction, and to study to the effect of these changes on the brain.

Funding: the lead author is funded by Medical Research Council Confidence in Concept Funding.

Table 3. *Summary of published MRI BBB water exchange techniques and measured k_{in} and PS_w in healthy rodent and human brain tissue. Values of PS_w and ki_n were reported where available. When values for both parameters were not available (i.e. in ASL based approaches), k_{in} or more typically PS_w were calculated using the following values for v_b: gray matter = 0.05 mL mL^{-1}. white matter = 0.03 mL mL^{-1}, whole brain = 0.04 mL mL^{-1}, contra-lateral hemisphere = 0.05 mL mL^{-1}. Calculated values are denoted with †.*

Author	***Technique***	***Sequence***	***Acquisition parameters***	***Subjects***	***k_{in} (min^{-1})***	***PS_w (mL min^{-1} mL^{-1})***	***Kinetic model***
Contrast agent based methods							
Schwarzbauer et al. (1997)[26]	*Dose ramping*	*2D IR turboFLASH*	*7T, axial, TR/TE = 2.6/1.4 ms, σ = 5°, TI = n*170ms (n = 1-16), voxel size = 0.27 x 0.55 x 2 mm, single slice, NSA = 16, Gd-DTPA-Polylysine*	*5 healthy female Lewis rats*	*207 (cortex) 102 (hippocampus) 638 (jaw muscle)*	*3.31 (cortex) 3.37 (hippocampus) 10.6 (jaw muscle)*	*Simplified 2CXM*
Kim et al. (2008)[29]	*Water exchange index (WEI)*	*3D SPGR*	*9.4T, axial, TR/TE = 40/4 ms, σ = 20°, 40°, 60°, 90°, voxel size = 0.25 x 0.25 x 0.25 mm, Gd-PGC*	*5 healthy male mice, aged 8 wo*	*N/A*	*N/A*	*Blood volume model*
Anderson et al. (2013)[27]	*First pass*	*2D TurboFLASH*	*7T, axial, TR/TE = unreported, flip angle = unreported, FOV = unreported, matrix = unreported, gadoteriodol*	*71 yo female with early AD*	*186 (WM)*	*2.3 (WM)*	*Simplified 2CXM*
Rooney et al. (2015)[28]	*First pass*	*2D inversion-recovery turboFLASH*	*7T, axial, σ = 6°, TI = 8 TI values (actual values not reported), voxel size = 2 x 2 x 10 mm, single slice, gadoteriodol*	*6 healthy humans (4 female, 2 male), aged 30 yo*	*146 (GM), 171 (WM)*	*4.5 (GM), 2.4 (WM)*	*Simplified 2CXM*
Dickie et al. (2019)[31]	*Multi-flip angle multi-echo (MFAME)-MRI*	*3D multi-gradient echo SPGR*	*7T, axial, TR/TE = 100/2 ms 10 echoes; ΔTE = 2 ms, σ = 10°, 20°, 30°, 40°, 80°, voxel size = 0.94 x 0.94 x 0.94 mm, 30 slices, Gd-DOTA*	*5 healthy male Fisher 344 rats aged 18 mo*	*171 (hippocampus) 70 (cortex) 128 (striatum) 42 (thalamus) *unpublished data*	*4.9 (hippocampus) 2.7 (cortex) 3.5 (striatum) 2.6 (thalamus)*	*2CXM*

Zaharchuk et al. (1998)[76]	*CAPTIVE MRI*	*Pre- and post-contrast ASL*	*4.7T, axial, TR/TE = 4000/40ms, voxel size = 0.78 x 0.78 x 2 mm, single slice, pulse duration = 3.7s, PLD = 0.2s, MPEG-PL-Dy-DTPA*	*10 healthy Sprague Dawley rats*	*72 (striatum)†*	*2.9 (striatum)*	*2CXM*
Beaumont et al. (2016)[77]	*Contrast-enhanced ASL*	*Pre- and post-contrast ASL (STAR with look-locker readout)*	*3T, axial, TR/TE = 4000/11 ms, voxel size = 3.5 x 3.5 x 7 mm, 11 slices, slice gap = 1mm, 11 PLDs = 300-3300 ms, NEX = 60*	*1 healthy human subject*	*38 (GM)*	*1.5 (GM)†*	*2CXM*
Non-contrast agent methods							
Parkes et al. (2002)[43]	*ASL*	*CASL with GE-EPI*	*1.5T, TR/TE = 4000/34 ms, voxel size = 3.75 x 3.75 x 7 mm, 7 slices, PLDs = 0-1500 ms, labeling duration = 1.7s, NEX = 45*	*3 healthy female humans, mean age 28 yo*	*19 (GM), 2.9 (WM)*	*0.95 (GM)†, 0.087 (WM)†*	*2CXM*
Li et al. (2007)[51]	*ASL*	*PASL with DIPLOMA*	*1.5T, TR/TE = 2500/15 ms, voxel size = 3.7 x 2.3 x 8 mm, 5 slices ,slice gap = 2mm, 11 PLDs = 300 – 3000 ms*	*8 healthy humans aged between 24-80 yo*	*420.7 (cortical GM)*	*12.6 (cortical GM)†*	*Four-phase single capillary stepwise*
Carr et al. (2007)[41]	*ASL*	*FAIR*	*9.4T, voxel size = not reported. single slice, slice thickness = 2 mm, 7 PLDs = 1000-5000 ms, NEX = 6*	*4 healthy rats*	*Not measurable*	*Not measurable*	*2CXM*
Wells et al. (2013)[47]	*Multi-TE ASL*	*PASL (FAIR) with two-shot segmented SE-EPI*	*9.4T, TR = 2500/19-60 ms, 16 TEs, voxel size = 0.55 x 0.55 x 2 mm, single slice, NEX = 5, PLDs = 1000, 1500, 2000, 2500 ms*	*9 healthy male Sprague Dawley rats*	*162 (cortex) *calculated by taking the inverse of T_{ex}*	*8.1 (cortex)†*	*Kety + vascular compartment*
Gregori et al. (2013)[48]	*Multi-TE ASL*	*PCASL (FAIR) with 3D GRASE*	*3T, axial, TR = 3800 ms, TEs = 16.5, 49.4, 82.3, 20, voxel size = 3 x 3 x 4 mm, 26 slice, PLDs =150-3000 ms*	*5 healthy human volunteers aged between 24 and 36 yo*	*137 (GM)*	*6.9 (GM)†*	*Kety + vascular compartment*

Ohene et al. (2018)[115]	*Multi-TE ASL*	*PCASL (FAIR) with segmented 2D SE-EPI*	*9.4T, axial, TR = 5000 ms, TEs = 15, 23, 30, 40, 50, 65 ms, voxel size = 0.78 x 0.78 x 16 mm, single slice, PLDs = 400, 1000, 1500, 3500 ms, NEX = 20*	*9 male C57/BL6 mice aged 6 mo*	*174 (cortex) *calculated by taking the inverse of T_{ex}*	*8.7 (cortex)†*	*Kety + vascular compartment*
Silva et al. (1997a)[70]	*Diffusion weighted ASL*	*Adiabatic fast passage inversion ASL with PGSE*	*4.7T, TE = 47 ms, PLD = 0, b = 0 – 1739 in 12 steps, no in plane location, label duration = 3.5 s*	*12 healthy male Sprague-Dawley rats*	*70 (whole brain)†*	*2.8 (whole brain) *calculated from E = 0.85 and CBF = 145 mL min^{-1} g^{-1}*	*IVIM f assumed to be equal to E*
Wang et al. (2007)[71]	*Diffusion weighted ASL*	*Amplitude modulated DW-CASL*	*3T, axial, TR/TE = 4000-4500/55-60 ms, voxel size = 3.4 x 3.4 x 8 mm, 6 slices, PLDs = 0.8, 1.2, 1.5 s, b=0, 10, 25, 50, 100, 150, 200, 300 s mm^2*	*13 healthy humans (6 women, 7 men) aged 26.4 yo*	*193 (GM)*	*9.7 (GM)†*	*SPA (compartment model version)*
St. Lawrence et al. (2012)[72]	*Diffusion weighted ASL*	*Balanced DW- pCASL*	*3T, axial, TR/TE = 4000/48 ms voxel size = 3.4 x 3.4 x 8 mm, 8 slices, PLD = 1500 ms, b = 0, 50 s/mm^2*	*7 healthy human subjects (3 female, 4 male) aged 28 yo*	*139 (GM), 154 (WM)*	*7.0 (GM)†, 4.6 (WM)†*	*SPA (compartment model version)*
Palomares et al. (2016)[96]	*Diffusion weighted ASL*	*DW-pCASL*	*3T, axial, TR/TE = 4300/47 ms, voxel size = 3.6 x 3.6 x 3.5 mm, 38 slices, PLD = 1500 ms, NEX = 80, b = 0, 50 s/mm^2*	*9 healthy human subjects (4 female, 5 male) aged 38.8 yo*	*221 (GM), 261 (WM)*	*11 (GM)†, 7.8 (WM)†*	*SPA (compartment model version)*
Tiwari et al. (2017)[94]	*Diffusion weighted ASL*	*DW-pCASL*	*7T, TR/TE = 3000/28ms, 4 x 4 x 3 mm, 4 slices, PLD = 400 ms, NEX = 60, b values = 0, 50 s mm^{-2} (along z)*	*12 male healthy Sprague Dawley rats aged 8-10 wo*	*363 (contra-lesional hemisphere)*	*18 (contra-lesional hemisphere)†*	*SPA (compartment model version)*
Shao et al. (2018)[116]	*Diffusion weighted ASL*	*DW-pCASL with 3D GRASE*	*3T, axial, TR/TE = 4000/36.5 ms, voxel size = 3.5 x 3.5 x 8 mm, slices = 12, b = 50 s mm^{-2}, PLD = 1800 ms*	*19 elderly subjects (7 male, 12 female), mean age 68.8 yo*	*109 (GM), 94.1 (WM)*	*5.5 (GM)†, 2.8 (WM)†*	*Regularised SPA*
Wengler et al. (2019)[74]	*Intrinsic diffusivity encoding of*	*pCASL with 3D segmented GRASE*	*3T, axial, TR/TE = 4500/16 ms, σ = 120°, voxel size = 4 x 4 x 4 mm, PAR turbo factors of 12 and 48, PLD = 2000 m.*	*15 healthy subjects (8 male, 7 female)*	*171 (GM) 146 (WM) *using τ_b = 350 ms and 410 ms*	*1.3 (GM) 0.76 (GM)*	*Regularised SPA*

	arterial labelled spin (IDEALS)				*respectively as per paper*		
Silva et al. (1997b)[75]	*Magnetisation transfer weighted ASL*	*Volume localised STEAM*	*4.7T, coronal, TR = unreported, TE = 30 ms, voxel size = unreported,*	*25 healthy Sprague Dawley rats*	*Not measured*	*Not measured*	*2CXM*
Hales et al.[117]	*IVIM + ASL*	*Separate 2D EPI (diffusion) and pCASL (FAIR) with GRASE readout (ASL)*	*1.5T, axial, voxel size = 3.6 x 3.6 x 5 mm, 20 slices, NEX = 8.* *ASL: TR/TE = 3000/31.6 ms, PLDs = 0.2, 0.4, 0.6, 0.8, 1.0, 1.2, 1.4, 1.6, 1.8, 2.0, 2.2, 2.4 s.* *DW-MRI: TR/TE = 3800/120, b = 0, 20, 40, 80, 120, , 160, 200, 300, 500, 1000 s/mm^2*	*10 healthy human subjects (4 female, 6 male) mean age 27 years*	*48 (GM)†*	*1.1 (GM)*	*IVIM (diffusion data) and four-phase single capillary stepwise model (ASL data)*
Lin et al. (2018)[118]	*Phase-contrast (WEPCAST) ASL*	*ASL with phase-contrast velocity-encoding gradients*	*3T, sagittal, TR/TE = 7546/9.2 ms, voxel size = 3.1 x 3.1 x 10, single slice placed midway through the brain, PLDs = 1500, 2000, 2500, 3000, 3500, 4000, 4500, and 5000 ms, label duration = 2000 ms, V_{enc} = 15cm/s, NEX = 10*	*6 healthy human participants (3 female, 3 male) mean age 27 years*	*38 (whole brain)†*	*1.9 (whole brain)*	*Venous model incorporating extraction and dispersion*

Table 4. *Mean k_{in} (and s.e.m) and PS_w (and s.e.m) in healthy human and rodent brain. Data from Li et al.* [51] *and Tiwari et al.* [94] *were treated as extreme values and excluded. When not measured, values for PS_w were calculated as described in the legend of Table 3.*

	Human gray matter (n = 7)	***Human white matter (n = 5)***	***Rodent gray matter (n = 4)***
k_{in} (min^{-1})	*159 (14)*	*165 (27)*	*148 (16)*
PS_w ($mL\ min^{-1}\ mL^{-1}$)	*6.6 (1.2)*	*3.6 (1.4)*	*5.9 (1.5)*

Table 5. Blood-brain barrier water exchange measurements in pathological brain tissue

Author	***MRI Technique***	***Subjects***	***Findings***
Li et al. (2005)	*ASL*	*Healthy subjects with different ages (n = 8)*	*Trend towards decreasing k_w with age*
Kim et al. (2008)[29]	*Water exchange index*	*Surgical model of middle cerebral artery occlusion (MCAo) in male C57BL/6 mice (n = 5) and controls (n = 4).*	*WEI elevated in ipsilesional cortex between 1-4 hours after MCAo*
Huang et al. (2013)[60]	*Water exchange index*	*Acute transient stroke model in male C57BL/6 mice (stroke, n = 15; controls, n = 6)*	*WEI in ipsilesional cortex increased by 1.97 in controls to 4.67 in stroke mice. Approximately 33% of mice did not exhibit any change however.*
Dickie et al. (2019)[31]	*MFAME-MRI*	*Transgenic rat model of Alzheimer's disease (n = 7 TgF344-AD, n = 5 wild-types).*	*PS_w increased in AD rats relative to wild-types (k_{in} increased in AD rats – results not published).*
Rooney et al. (2015)[28]	*Dose-ramping CE-MRI*	*Patients with glioblastoma (n = 5, 3M/2F, 19–57 years)*	*k_{in} reduced in tumour (k_{in} < 10 min^{-1}) relative to normal appearing grey matter (k_{in} = 192 min^{-1}).*
Wang et al. (2007)[71]	*DW-ASL*	*Patient with brain tumour (n = 1, grade II oligodendroglioma)*	*k_{in} increased in tumour (k_{in} = 463 min^{-1}) relative to normal appearing grey matter (k_{in} = 224 min^{-1}).*
Rooney et al. (2015)[28]	*First-pass CE-MRI*	*Relapsing remitting multiple sclerosis (n = 6, 2M/4F, 46 (±7) years, 18–55 years)*	*k_{in} reduced in NAGM (k_{in} = 120 min^{-1}), NAWM (k_{in} = 132 min^{-1}), and lesion (k_{in} = 108 min^{-1}) relative to healthy controls (GM; k_{in} = 174 min^{-1}, WM; k_{in} = 186 min^{-1})*
Palomares et al (2016)[96]	*DW-ASL*	*Participants with obstructive sleep apnea (n = 9) and controls (n = 9)*	*k_{in} reduced in persons with sleep apnea (GM; k_{in} = 158 min^{-1}, WM; k_{in} = 178 min^{-1}) relative to controls (GM; k_{in} = 221 min^{-1}, WM; k_{in} = 261 min^{-1}).*
Shao et al. (2018)[116]	*DW-ASL*	*Elderly patients at risk of small vessel disease (n = 19)*	*k_{in} increased in type-2 diabetes (28.2% increase), hypercholestremia (19.5% increase), and with vascular risk (~12% increase). k_{in} also predicted sum of box and clinical dementia ratings.*

Table 6. *Rodent validation studies*				
Author	***Validation method***	***MRI technique***	***Subjects***	***Findings***
Huang et al. (2013)[60]	*Mannitol and hypercapnic challenge*	*Water exchange index*	*Male C57BL/6 mice (mannitol, n = 7; CO_2, n = 6)*	*Mannitol increased WEI and CBV as early as 15 minutes post injection. Hypercapnia (2.5%-10% CO_2) also increased WEI and CBV.*
Zaharchuk et al. (1998)[76]	*Hypercapnic challenge*	*CAPTIVE MRI*	*Sprague Dawley rats (n = 10)*	*Hypercapnia reduced extraction fraction. PS_w unaffected.*
Silva et al. (1997a)[70]	*Hypercapnic challenge*	*Diffusion weighted ASL*	*Male Sprague Dawley rats (n = 12)*	*Hypercapnia reduced extraction fraction.*
Silva et al. (1997b)[75]	*Mannitol challenge*	*Magnetisation transfer weighted ASL*	*Sprague Dawley rats (n = 7)*	*Mannitol increased water-extraction fraction*
Dickie et al. (2019)[31]	*Immunofluorescence staining for occludin, claudin-5, aquaporin-4 and lectin.*	*MFAME-MRI*	*Transgenic Alzheimer's disease rats (TgF344-AD, n = 7) and wild-types (n = 5)*	*Significant inverse correlation between PS_w and tight junction protein expression (occludin).*
Ohene et al. (2019)[115]	*AQP4-null knockout mice*	*Multi-TE ASL*	*Male AQP4 null mice (n = 9) and C57/BL6 wild-types (n = 9)*	*Significant reduction in k_{in} in AQP4 null mice relative to wild-types (132 min^{-1} versus 172 min^{-1})*

Bibliography

[1] A. Armulik, G. Genové, M. Mäe, M.H. Nisancioglu, E. Wallgard, C. Niaudet, L. He, J. Norlin, P. Lindblom, K. Strittmatter, B.R. Johansson, C. Betsholtz, Pericytes regulate the blood-brain barrier., Nature. 468 (2010) 557–561. doi:10.1038/nature09522.

[2] R. Daneman, L. Zhou, A.A. Kebede, B.A. Barres, Pericytes are required for blood-brain barrier integrity during embryogenesis, Nature. 468 (2010) 562–566. doi:10.1038/nature09513.

[3] G. Li, W. Yuan, B.M. Fu, A model for the blood-brain barrier permeability to water and small solutes, J. Biomech. 43 (2010) 2133–2140. doi:10.1016/j.jbiomech.2010.03.047.

[4] P. Beard, Biomedical photoacoustic imaging, Interface Focus. 1 (2011) 602–631. doi:10.1098/rsfs.2011.0028.

[5] M. Piert, R. a Koeppe, B. Giordani, S. Berent, D.E. Kuhl, Diminished glucose transport and phosphorylation in Alzheimer's disease determined by dynamic FDG-PET., J. Nucl. Med. 37 (1996) 201–208.

[6] S. Syvänen, J. Eriksson, Advances in PET imaging of P-glycoprotein function at the blood-brain barrier, ACS Chem. Neurosci. 4 (2013) 225–237. doi:10.1021/cn3001729.

[7] F.A. Nasrallah, G. Pagès, P.W. Kuchel, X. Golay, K.H. Chuang, Imaging brain deoxyglucose uptake and metabolism by glucoCEST MRI, J. Cereb. Blood Flow Metab. 33 (2013) 1270–1278. doi:10.1038/jcbfm.2013.79.

[8] A.K. Heye, R.D. Culling, M. del C. Valdés Hernández, M.J. Thrippleton, J.M. Wardlaw, Assessment of blood–brain barrier disruption using dynamic contrast-enhanced MRI. A systematic review, NeuroImage Clin. 6 (2014) 262–274. doi:10.1016/j.nicl.2014.09.002.

[9] A.K. Heye, M.J. Thrippleton, P.A. Armitage, M. del C. Valdés Hernández, S.D. Makin, A. Glatz, E. Sakka, J.M. Wardlaw, Tracer kinetic modelling for DCE-MRI quantification of subtle blood-brain barrier permeability, Neuroimage. 125 (2016) 446–455. doi:10.1016/j.neuroimage.2015.10.018.

[10] P.A. Armitage, A.J. Farrall, T.K. Carpenter, F.N. Doubal, J.M. Wardlaw, Use of

dynamic contrast-enhanced MRI to measure subtle blood–brain barrier abnormalities, Magn. Reson. Imaging. 29 (2011) 305–314. doi:10.1016/j.mri.2010.09.002.

[11] T. Nitta, M. Hata, S. Gotoh, Y. Seo, H. Sasaki, N. Hashimoto, M. Furuse, S. Tsukita, Size-selective loosening of the blood-brain barrier in claudin-5-deficient mice, J. Cell Biol. 161 (2003) 653–660. doi:10.1083/jcb.200302070.

[12] H. Fischer, R. Gottschlich, A. Seelig, Blood-brain barrier permeation: Molecular parameters governing passive diffusion, J. Membr. Biol. 165 (1998) 201–211. doi:10.1007/s002329900434.

[13] J.O. Eichling, M.E. Raichle, R.L. Grubb, M.M. Ter Pogossian, Evidence of the limitations of water as a freely diffusible tracer in brain of the rhesus monkey, Circ. Res. 35 (1974) 358–364. doi:10.1161/01.RES.35.3.358.

[14] T.G. Bolwig, N.A. Lassen, The Diffusion Permeability to Water of the Rat Blood-Brain Barrier, Acta Physiol. Scand. 93 (1975) 415–422. doi:10.1111/j.1748-1716.1975.tb05831.x.

[15] O.. Paulson, M.. Hertz, T.. Bolwig, N.. Lassen, Filtration and Diffusion of Water Across Brain Barrier in Man, Microvasc. Res. 124 (1977) 113–123.

[16] W.M. Pardridge, G. Fierer, Blood-Brain Barrier Transport of Butanol and Water Relative to N-Isopropyl-p-iodoamphetamine as the Internal Reference, J. Cereb. Blood Flow Metab. 5 (1985) 275–281.

[17] S. Takagi, K. Ehara, R.D. Finn, Water extraction fraction and permeability-surface product after intravenous injection in rats, Stroke. 18 (1987) 177–183. doi:10.1161/01.STR.18.1.177.

[18] P. Herscovitch, M.E. Raichle, M.R. Kilbourn, M.J. Welch, Positron emission tomographic measurement of cerebral blood flow and permeability-surface area product of water using and 2 over black square]; [1 and 2 over black square]5O]water and and 2 over black square]; [1 and 2 over black square]1C]butanol, J. Cereb. Blood Flow Metab. 7 (1987) 527–542.

[19] T. Zeuthen, Water-Transporting Proteins, (2010) 57–73. doi:10.1007/s00232-009-

9216-y.

[20] C. Crone, The Permeability of Capillaries in Various Organs as Determined by Use of the ???Indicator Diffusion??? Method, Acta Physiol. Scand. 58 (1963) 292–305. doi:10.1111/j.1748-1716.1963.tb02652.x.

[21] E. Renkin, Transport of potassium-42 from blood to tissue in isolated mammalian skeletal muscles, Am J Physiol. 197 (1959) 1205–1210. http://ajplegacy.physiology.org/content/197/6/1205.abstract%5Cnhttp://ajplegacy.physiology.org/content/197/6/1205.abstract?sid=586b9277-9912-41a8-93a4-2e126ea90447.

[22] M.S. Berridge, L.P. Adler, A.D. Nelson, E.H. Cassidy, R.F. Muzic, E.M. Bednarczyk, F. Miraldi, Measurement of human cerebral blood flow with [15O]butanol and positron emission tomography, J. Cereb. Blood Flow Metab. 11 (1991) 707–715. doi:10.1038/jcbfm.1991.127.

[23] M.E. Raichle, J.O. Eichling, M.G. Straatmann, M.J. Welsh, K.B. Larson, M.M. Ter-Pogossian, Blood-brain barrier permeability alcohols and 150-labeled water, Am. J. Physiol. 230 (1976).

[24] M.E. Fabry, M. Eisenstadt, Water exchange between red cells and plasma. Measurement by nuclear magnetic relaxation, Biophys. J. 15 (1975) 1101–1110. doi:10.1016/S0006-3495(75)85886-3.

[25] T. Conlon, R. Outhred, Water diffusion permeability of erythrocytes using an NMR technique, BBA - Biomembr. 288 (1972) 354–361. doi:10.1016/0005-2736(72)90256-8.

[26] C. Schwarzbauer, S.P. Morrissey, R. Deichmann, C. Hillenbrand, J. Syha, H. Adolf, U. Nöth, A. Haase, Quantitative magnetic resonance imaging of capillary water permeability and regional blood volume with an intravascular {MR} contrast agent., Magn Reson Med. 37 (1997) 769–777.

[27] V.C. Anderson, D.P. Lenar, J.F. Quinn, W.D. Rooney, The blood-brain barrier and microvascular water exchange in Alzheimer’s disease., Cardiovasc. Psychiatry

Neurol. 2011 (2011) 615829. doi:10.1155/2011/615829.

[28] W.D. Rooney, X. Li, M.K. Sammi, D.N. Bourdette, E. a Neuwelt, C.S. Springer, Mapping human brain capillary water lifetime: high-resolution metabolic neuroimaging., NMR Biomed. 28 (2015) 607–23. doi:10.1002/nbm.3294.

[29] Y.R. Kim, E. Tejima, S. Huang, D.N. Atochin, G. Dai, E.H. Lo, P.L. Huang, A. Bogdanov, B.R. Rosen, In vivo quantification of transvascular water exchange during the acute phase of permanent stroke., Magn. Reson. Med. 60 (2008) 813–21. doi:10.1002/mrm.21708.

[30] S. Huang, C.T. Farrar, G. Dai, S.J. Kwon, A.A. Bogdanov, B.R. Rosen, Y.R. Kim, Dynamic monitoring of blood-brain barrier integrity using water exchange index (WEI) during mannitol and CO2 challenges in mouse brain, NMR Biomed. 26 (2013) 376–385. doi:10.1002/nbm.2871.

[31] B.R. Dickie, M. Vandesquille, J. Ulloa, H. Boutin, L.M. Parkes, G.J.M. Parker, Water-exchange MRI detects subtle blood-brain barrier breakdown in Alzheimer's disease rats, Neuroimage. (2019). doi:10.1016/j.neuroimage.2018.09.030.

[32] C.S. Landis, X. Li, F.W. Telang, P.E. Molina, I. Palyka, G. Vetek, C.S. Springer, Equilibrium transcytolemmal water-exchange kinetics in skeletal muscle in vivo, Magn. Reson. Med. 42 (1999) 467–478. doi:10.1002/(SICI)1522-2594(199909)42:3<467::AID-MRM9>3.0.CO;2-0.

[33] C.S. Springer, W.D. Rooney, X. Li, The effects of equilibrium transcytolemmal water exchange on the determination of contrast reagent concentration in vivo, Magn. Reson. Med. 47 (2002) 422–424. doi:10.1002/mrm.10099.

[34] D.L. Buckley, Shutter-speed dynamic contrast-enhanced MRI: Is it fit for purpose?, Magn. Reson. Med. 81 (2019) 976–988. doi:10.1002/mrm.27456.

[35] E.L. Barbier, K.S. St Lawrence, E. Grillon, A.P. Koretsky, M. Décorps, A model of blood-brain barrier permeability to water: accounting for blood inflow and longitudinal relaxation effects., Magn. Reson. Med. 47 (2002) 1100–9. doi:10.1002/mrm.10158.

[36] S.S. Kety, The theory and applications of the exchange of inert gas at the lungs and

tissues., Pharmacol. Rev. 3 (1951) 1–41. http://www.ncbi.nlm.nih.gov/pubmed/14833874.

[37] D.S. Williams, J.A. Detre, J.S. Leigh, A.P. Koretsky, Magnetic resonance imaging of perfusion using spin inversion of arterial water., Proc. Natl. Acad. Sci. U. S. A. 89 (1992) 212–6. doi:10.1073/pnas.89.9.4220e.

[38] Parkes, Tofts, Improved accuracy of human cerebral blood perfusion measurements using arterial spin labeling: Accounting for capillary water permeability, Magn. Reson. Med. 48 (2002) 27–41. doi:10.1002/mrm.10180.

[39] C.W. Wu, H.L. Liu, J.H. Chen, Y. Yang, Effects of CBV, CBF, and blood-brain barrier permeability on accuracy of PASL and VASO measurement, Magn. Reson. Med. 63 (2010) 601–608. doi:10.1002/mrm.22165.

[40] K.S. St Lawrence, J.A. Frank, A.C. McLaughlin, Effect of restricted water exchange on cerebral blood flow values calculated with arterial spin tagging: A theoretical investigation, Magn. Reson. Med. 44 (2000) 440–449. doi:10.1002/1522-2594(200009)44:3<440::AID-MRM15>3.0.CO;2-6.

[41] J.P. Carr, D.L. Buckley, J. Tessier, G.J.M. Parker, What levels of precision are achievable for quantification of perfusion and capillary permeability surface area product using ASL?, Magn. Reson. Med. 58 (2007) 281–289. doi:10.1002/mrm.21317.

[42] J. Zhou, D.A. Wilson, J.A. Ulatowski, R.J. Traystman, P.C. van Zijl, Two-compartment exchange model for perfusion quantification using arterial spin tagging., J. Cereb. Blood Flow Metab. 21 (2001) 440–455. doi:10.1097/00004647-200104000-00013.

[43] L.M. Parkes, P.S. Tofts, Improved accuracy of human cerebral blood perfusion measurements using arterial spin labeling: Accounting for capillary water permeability, Magn. Reson. Med. 48 (2002) 27–41. doi:10.1002/mrm.10180.

[44] L.. Parkes, Quantification of Cerebral Perfusion Using Arterial Spin Labeling: Two-Compartment Models, J. Magn. Reson. Imaging. 22 (2005) 732–736. doi:10.1002/jmri.20456.

[45] K.S. St Lawrence, T.Y. Lee, An adiabatic approximation to the tissue homogeneity model for water exchange in the brain: I. Theoretical derivation, J. Cereb. Blood Flow Metab. Off. J. Int. Soc. Cereb. Blood Flow Metab. 18 (1998) 1365–1377. doi:10.1097/00004647-199812000-00011.

[46] D.C. Alsop, J.A. Detre, Reduced transit-time sensitivity in noninvasive magnetic resonance imaging of human cerebral blood flow, J. Cereb. Blood Flow Metab. 16 (1996) 1236–1249. doi:10.1097/00004647-199611000-00019.

[47] J.A. Wells, B. Siow, M.F. Lythgoe, D.L. Thomas, Measuring biexponential transverse relaxation of the ASL signal at 9.4T to estimate arterial oxygen saturation and the time of exchange, J. Cereb. Blood Flow Metab. 33 (2013) 215–224. http://breast-cancer-research.biomedcentral.com/articles/10.1186/bcr807.

[48] J. Gregori, N. Schuff, R. Kern, M. Gunther, T2-based Arterial Spin Labeling measurements of blood to tissue water transfer in human brain, J. Magn. Reson. Imaging. 37 (2013) 332–342. doi:10.1002/bmb.20244.DNA.

[49] J. Johnson, T. Wilson, A model for capillary exchange., Am. J. Physiol. 210 (1966) 1299–303. doi:10.1152/ajplegacy.1966.210.6.1299.

[50] K.S. St. Lawrence, T.-Y. Lee, An Adiabatic Approximation to the Tissue Homogeneity Model for Water Exchange in the Brain: II. Experimental Validation, J. Cereb. Blood Flow Metab. 18 (1998) 1378–1385. doi:10.1097/00004647-199812000-00012.

[51] K. Li, X. Zhu, N. Hylton, G.-H. Jahng, M.W. Weiner, N. Schuff, Four-phase single-capillary stepwise model for kinetics in arterial spin labeling MRI., Magn. Reson. Med. 53 (2005) 511–8. doi:10.1002/mrm.20390.

[52] G.J. Stanisz, E.E. Odrobina, J. Pun, M. Escaravage, S.J. Graham, M.J. Bronskill, R.M. Henkelman, T1, T2 relaxation and magnetization transfer in tissue at 3T, Magn. Reson. Med. 54 (2005) 507–512. doi:10.1002/mrm.20605.

[53] X. Zhang, E.T. Petersen, E. Ghariq, J.B. De Vis, A.G. Webb, W.M. Teeuwisse, J. Hendrikse, M.J.P. Van Osch, In vivo blood T1 measurements at 1.5 T, 3 T, and 7 T, Magn. Reson. Med. 70 (2013) 1082–1086. doi:10.1002/mrm.24550.

[54] H.J. van de Haar, S. Burgmans, J.F.A. Jansen, M.J.P. van Osch, M.A. van Buchem, M. Muller, P.A.M. Hofman, F.R.J. Verhey, W.H. Backes, Blood-Brain Barrier Leakage in Patients with Early Alzheimer Disease, Radiology. 281 (2016) 527–535. doi:10.1148/radiol.2016152244.

[55] Y.X.J. Wáng, J.-M. Idée, A comprehensive literatures update of clinical researches of superparamagnetic resonance iron oxide nanoparticles for magnetic resonance imaging, Quant. Imaging Med. Surg. 7 (2017) 88–122. doi:10.21037/qims.2017.05.05.

[56] K.M. Donahue, R.M. Weisskoff, D. Burstein, Water diffusion and exchange as they influence contrast enhancement, J. Magn. Reson. Imaging. 7 (1997) 102–110. doi:10.1002/jmri.1880070114.

[57] W. Shin, T.A. Cashen, S.W. Horowitz, R. Sawlani, T.J. Carroll, Quantitative CBV measurement from static T1 changes in tissue and correction for intravascular water exchange., Magn. Reson. Med. 56 (2006) 138–145. doi:10.1002/mrm.20937.

[58] Y.R. Kim, K.J. Rebro, K.M. Schmainda, Water exchange and inflow affect the accuracy of T1-GRE blood volume measurements: implications for the evaluation of tumor angiogenesis, Magn Reson Med. 47 (2002) 1110–1120. doi:10.1002/mrm.10175.

[59] G.R. Moran, F.S. Prato, Modeling (1H) exchange: an estimate of the error introduced in MRI by assuming the fast exchange limit in bolus tracking, Magn Reson Med. 51 (2004) 816–827. doi:10.1002/mrm.20002.

[60] S. Huang, J.K. Kim, D.N. Atochin, C.T. Farrar, P.L. Huang, J.Y. Suh, S.J. Kwon, W.H. Shim, H. Cho, G. Cho, Y.R. Kim, Cerebral blood volume affects blood-brain barrier integrity in an acute transient stroke model., J. Cereb. Blood Flow Metab. 33 (2013) 898–905. doi:10.1038/jcbfm.2013.27.

[61] J.A. Wells, M.F. Lythgoe, M. Choy, D.G. Gadian, R.J. Ordidge, D.L. Thomas, Characterizing the origin of the arterial spin labelling signal in MRI using a multiecho acquisition approach, J Cereb Blood Flow Metab. 29 (2009) 1836–1845. doi:10.1038/jcbfm.2009.99.

[62] L. Hirschler, L.P. Munting, A. Khmelinskii, W.M. Teeuwisse, E. Suidgeest, J.M. Warnking, L. van der Weerd, E.L. Barbier, M.J.P. van Osch, Transit time mapping in the mouse brain using time-encoded pCASL, NMR Biomed. 31 (2018) 1–11. doi:10.1002/nbm.3855.

[63] J.P. Wansapura, S.K. Holland, R.S. Dunn, W.S. Ball, NMR Relaxation Times in the HumanBrain at 3.0 Tesla, J. Magn. Reson. Imaging. 538 (1999) 531–538.

[64] E. Cox, P.A. Gowland, Measuring T2 and T2' in the brain at 1.5T, 3T and 7T using a hybrid gradient echo-spin echo sequence and EPI, Proc. Intl. Soc. Mag. Reson. Med. Toronto (2008) 1411. /MyPathway2008/1411.

[65] L.C. Krishnamurthy, P. Liu, F. Xu, J. Uh, I. Dimitrov, H. Lu, Dependence of blood T2 on oxygenation at 7 T: In vitro calibration and in vivo application, Magn. Reson. Med. 71 (2014) 2035–2042. doi:10.1002/mrm.24868.

[66] J.M. Zhao, C.S. Clingman, M.J. Närväinen, R.A. Kauppinen, P.C.M. Van Zijl, Oxygenation and hematocrit dependence of transverse relaxation rates of blood at 3T, Magn. Reson. Med. 58 (2007) 592–597. doi:10.1002/mrm.21342.

[67] M.J. Silvennoinen, C.S. Clingman, X. Golay, R.A. Kauppinen, P.C.M. Van Zijl, Comparison of the dependence of blood R2 and R2* on oxygen saturation at 1.5 and 4.7 Tesla, Magn. Reson. Med. 49 (2003) 47–60. doi:10.1002/mrm.10355.

[68] J.A. Wells, B. Siow, M.F. Lythgoe, D.L. Thomas, Measuring biexponential transverse relaxation of the ASL signal at 9.4 T to estimate arterial oxygen saturation and the time of exchange of labeled blood water into cortical brain tissue, J. Cereb. Blood Flow Metab. 33 (2013) 215–224. doi:10.1038/jcbfm.2012.156.

[69] D. Le Bihan, E. Breton, D. Lallemand, M.L. Aubin, J. Vignaud, M. Laval-Jeantet, Separation of diffusion and perfusion in intravoxel incoherent motion MR imaging., Radiology. 168 (1988) 497–505. doi:10.1148/radiology.168.2.3393671.

[70] A.C. Silva, D.S. Williams, A.P. Koretsky, Evidence for the exchange of arterial spin-labeled water with tissue water in rat brain from diffusion-sensitized measurements of perfusion., Magn. Reson. Med. 38 (1997) 232–7. doi:10.1002/mrm.1910380211.

[71] J. Wang, M.A. Fernández-Seara, S. Wang, K.S.S. Lawrence, When Perfusion Meets Diffusion: *in vivo* Measurement of Water Permeability in Human Brain, J. Cereb. Blood Flow Metab. 27 (2007) 839–849. doi:10.1038/sj.jcbfm.9600398.

[72] K.S. St. Lawrence, D. Owen, D.J.J. Wang, A two-stage approach for measuring vascular water exchange and arterial transit time by diffusion-weighted perfusion MRI, Magn. Reson. Med. 67 (2012) 1275–1284. doi:10.1002/mrm.23104.

[73] J. Wang, D.C. Alsop, H.K. Song, J.A. Maldjian, K. Tang, A.E. Salvucci, J.A. Detre, Arterial transit time imaging with flow encoding arterial spin tagging (FEAST), Magn. Reson. Med. 50 (2003) 599–607. doi:10.1002/mrm.10559.

[74] K. Wengler, L. Bangiyev, T. Canli, T.Q. Duong, M.E. Schweitzer, X. He, 3D MRI of whole-brain water permeability with intrinsic diffusivity encoding of arterial labeled spin (IDEALS), Neuroimage. 189 (2019) 401–414. doi:10.1016/j.neuroimage.2019.01.035.

[75] A.C. Silva, W. Zhang, D.S. Williams, A.P. Koretsky, Estimation of water extraction fractions in rat brain using magnetic resonance measurement of perfusion with arterial spin labeling, Magn. Reson. Med. 37 (1997) 58–68. doi:10.1002/mrm.1910370110.

[76] G. Zaharchuk, A.A. Bogdanov, J.J.A. Marota, M. Shimizu-Sasamata, R.M. Weisskoff, K.K. Kwong, B.G. Jenkins, R. Weissleder, B.R. Rosen, Continuous Assessment of Perfusion by Tagging Including Volume and Water Extraction (CAPTIVE): A steady-state contrast agent technique for measuring blood flow, relative blood volume fraction, and the water extraction fraction, Magn. Reson. Med. 40 (1998) 666–678. doi:10.1002/mrm.1910400504.

[77] H. Beaumont, A. Pearson, M. Van Osch, L. Parkes, Estimation of Water Exchange across the Blood Brain Barrier Using Contrast-Enhanced ASL.", 24th Annu. Meet. Int. Soc. Magn. Reson. Med. (2016).

[78] Z. Lin, Y. Li, P. Su, D. Mao, Z. Wei, J.J. Pillai, A. Moghekar, M. van Osch, Y. Ge, H. Lu, Non-contrast MR imaging of blood-brain barrier permeability to water, Magn. Reson. Med. (2018) 1–14. doi:10.1002/mrm.27141.

[79] E.C. Wong, Vessel-encoded arterial spin-labeling using pseudocontinuous tagging,

Magn. Reson. Med. 58 (2007) 1086–1091. doi:10.1002/mrm.21293.

[80] J.J.H. Ackerman, C.S. Ewy, N.N. Becker, R.A. Shalwitz, Deuterium nuclear magnetic resonance measurements of blood flow and tissue perfusion employing 2H2O as a freely diffusible tracer., Proc. Natl. Acad. Sci. U. S. A. 84 (1987) 4099–4102. doi:10.1073/pnas.84.12.4099.

[81] F.N. Wang, S.L. Peng, C.T. Lu, H.H. Peng, T.C. Yeh, Water signal attenuation by D2O infusion as a novel contrast mechanism for1H perfusion MRI, NMR Biomed. 26 (2013) 692–698. doi:10.1002/nbm.2914.

[82] R.J.T. Corbett, A.R. Laptook, E. Olivares, Simultaneous measurement of cerebral blood flow and energy metabolites in piglets using deuterium and phosphorus nuclear magnetic resonance, J. Cereb. Blood Flow Metab. 11 (1991) 55–65. doi:10.1038/jcbfm.1991.6.

[83] H. Igarashi, V.J. Huber, M. Tsujita, T. Nakada, Pretreatment with a novel aquaporin 4 inhibitor, TGN-020, significantly reduces ischemic cerebral edema, Neurol. Sci. 32 (2011) 113–116. doi:10.1007/s10072-010-0431-1.

[84] H. Igarashi, Y. Suzuki, I.L. Kwee, T. Nakada, Water influx into cerebrospinal fluid is significantly reduced in senile plaque bearing transgenic mice, supporting beta-amyloid clearance hypothesis of Alzheimer's disease, Neurol. Res. 36 (2014) 1094–1098. doi:10.1179/1743132814Y.0000000434.

[85] V.J. Huber, H. Igarashi, S. Ueki, I.L. Kwee, T. Nakada, Aquaporin-4 facilitator TGN-073 promotes interstitial fluid circulation within the blood-brain barrier: [17 O]H 2 O JJVCPE MRI study, Neuroreport. 29 (2018) 697–703. doi:10.1097/WNR.0000000000000990.

[86] K. Kudo, T. Harada, H. Kameda, I. Uwano, F. Yamashita, S. Higuchi, K. Yoshioka, M. Sasaki, Indirect MRI of 17O-labeled water using steady-state sequences: Signal simulation and preclinical experiment, J. Magn. Reson. Imaging. 47 (2018) 1373–1379. doi:10.1002/jmri.25848.

[87] I. Ronen, H. Merkle, K. Ugurbil, G. Navon, Imaging of H217O distribution in the brain

of a live rat by using proton-detected 17O MRI, Proc. Natl. Acad. Sci. 95 (1998) 12934–12939.

[88] X.H. Zhu, N. Zhang, Y. Zhang, X. Zhang, K. Ugurbil, W. Chen, In vivo 17O NMR approaches for brain study at high field, NMR Biomed. 18 (2005) 83–103. doi:10.1002/nbm.930.

[89] I. Ronen, J.H. Lee, H. Merkle, K. Ugurbil, G. Navon, Imaging H2/17O distribution in a phantom and measurement of metabolically produced H2/17O in live mice by proton NMR, NMR Biomed. 10 (1997) 333–340. doi:10.1002/(SICI)1099-1492(199710)10:7<333::AID-NBM465>3.0.CO;2-E.

[90] K.K. Kwong, A.L. Hopkins, J.W. Belliveau, D.A. Chesler, L.M. Porkka, R.C. McKinstry, D.A. Finelli, G.J. Hunter, J.B. Moore, R.G. Barr, B.R. Rosen, Proton NMR imaging of cerebral blood flow using H217O, Magn. Reson. Med. 22 (1991) 154–158. doi:10.1002/mrm.1910220116.

[91] H. Igarashi, M. Tsujita, I.L. Kwee, T. Nakada, Water influx into cerebrospinal fluid is primarily controlled by aquaporin-4, not by aquaporin-1: 17O JJVCPE MRI study in knockout mice, Neuroreport. 25 (2014) 39–43. doi:10.1097/WNR.0000000000000042.

[92] A.L. Hopkins, E.M. Haacke, J. Tkach, R.G. Barr, C.B. Bratton, Improved sensitivity of proton MR to oxygen-17 as a contrast agent using fast imaging: Detection in brain, Magn. Reson. Med. 7 (1988) 222–229. doi:10.1002/mrm.1910070210.

[93] W.A. Anderson, J.T. Arnold, Proton relaxation times in H2O D2O mixtures, Phys. Rev. 101 (1956) 511–512. doi:10.1103/PhysRev.101.511.

[94] Y. V Tiwari, J. Lu, Q. Shen, B. Cerqueira, T.Q. Duong, Magnetic resonance imaging of blood–brain barrier permeability in ischemic stroke using diffusion-weighted arterial spin labeling in rats, J. Cereb. Blood Flow Metab. 37 (2017) 2706–2715. doi:10.1177/0271678X16673385.

[95] X. Shao, S.J. Ma, M. Casey, L. D'Orazio, J.M. Ringman, D.J.J. Wang, Mapping water exchange across the blood-brain barrier using 3D diffusion-prepared arterial spin labeled perfusion MRI, Magn. Reson. Med. (2018) 1–15. doi:10.1002/mrm.27632.

[96] J.A. Palomares, S. Tummala, D.J.J. Wang, B. Park, M.A. Woo, D.W. Kang, K.S.S. Lawrence, R.M. Harper, R. Kumar, Water Exchange across the Blood-Brain Barrier in Obstructive Sleep Apnea: An MRI Diffusion-Weighted Pseudo-Continuous Arterial Spin Labeling Study, J. Neuroimaging. 25 (2015) 900–905. doi:10.1111/jon.12288.

[97] Y. Zhang, M. Poirier-Quinot, C.S. Springer, J.A. Balschi, Active trans-plasma membrane water cycling in yeast is revealed by NMR, Biophys. J. 101 (2011) 2833–2842. doi:10.1016/j.bpj.2011.10.035.

[98] R. Bai, C.S. Springer, D. Plenz, P.J. Basser, Brain active transmembrane water cycling measured by MR is associated with neuronal activity, Magn. Reson. Med. (2018) 1–16. doi:10.1002/mrm.27473.

[99] R. Bai, C.S. Springer, D. Plenz, P.J. Basser, Fast, Na+/K+pump driven, steady-state transcytolemmal water exchange in neuronal tissue: A study of rat brain cortical cultures, Magn. Reson. Med. 79 (2018) 3207–3217. doi:10.1002/mrm.26980.

[100] Y. Ohene, I.F. Harrison, P. Nahavandi, O. Ismail, E. V. Bird, O.P. Ottersen, E.A. Nagelhus, D.L. Thomas, M.F. Lythgoe, J.A. Wells, Non-invasive MRI of brain clearance pathways using multiple echo time arterial spin labelling: An Aquaporin-4 study, Neuroimage. (2018). doi:10.1016/J.NEUROIMAGE.2018.12.026.

[101] H. Igarashi, M. Tsujita, Y. Suzuki, I.L. Kwee, T. Nakada, Inhibition of aquaporin-4 significantly increases regional cerebral blood flow, Neuroreport. 24 (2013) 324–328. doi:10.1097/WNR.0b013e32835fc827.

[102] D. Atochin, M. Litvak, S. Huang, Y.R. Kim, P. Huang, Role of eNOS in water exchange index maintenance-MRI studies, J. Phys. Conf. Ser. 886 (2017). doi:10.1088/1742-6596/886/1/012002.

[103] S.I. Rapoport, Osmotic opening of the blood-brain barrier: Principles, mechanism, and therapeutic applications, Cell. Mol. Neurobiol. 20 (2000) 217–230. doi:10.1023/A:1007049806660.

[104] C.N. Hall, C. Reynell, B. Gesslein, N.B. Hamilton, A. Mishra, B.A. Sutherland, F.M. O'Farrell, A.M. Buchan, M. Lauritzen, D. Attwell, Capillary pericytes regulate cerebral

blood flow in health and disease., Nature. 508 (2014) 55–60. doi:10.1038/nature13165.

[105] I.R. Cameron, H. Davson, M.B. Segal, The effect of hypercapnia on the blood-brain barrier to sucros in the rabbit, J. Biol. Med. 42 (1970) 241–247.

[106] C.A.. Evans, J.M. Reynolds, M.L. Reynolds, N.. Saunders, The effect of hypercapnia on a blood-brain barrier mechanism in foetal and new-born sheep, J. Physiol. 255 (1976) 701–714.

[107] M.D. Herbst, J.H. Goldstein, A review of water diffusion measurement by NMR in human red blood cells., Am. J. Physiol. 256 (1989) C1097-104. doi:10.1152/ajpcell.1989.256.5.C1097.

[108] D.M. Yang, J.E. Huettner, G.L. Bretthorst, J.J. Neil, J.R. Garbow, J.J.H. Ackerman, Intracellular water preexchange lifetime in neurons and astrocytes, Magn. Reson. Med. 79 (2018) 1616–1627. doi:10.1002/mrm.26781.

[109] E. Syková, C. Nicholson, Diffusion in Brain Extracellular Space, Physiol. Rev. 88 (2008) 1277–1340. doi:10.1152/physrev.00027.2007.

[110] J. Andrasko, Water diffusion permeability of human erythrocytes studied by a pulsed gradient NMR technique, BBA - Gen. Subj. 428 (1976) 304–311. doi:10.1016/0304-4165(76)90038-6.

[111] M. Nilsson, J. Lätt, D. Van Westen, S. Brockstedt, S. Lasič, F. Ståhlberg, D. Topgaard, Noninvasive mapping of water diffusional exchange in the human brain using filter-exchange imaging, Magn. Reson. Med. 69 (2013) 1573–1581. doi:10.1002/mrm.24395.

[112] G.T. Manley, M. Fujimura, T. Ma, N. Noshita, F. Filiz, A.W. Bollen, P. Chan, A.S. Verkman, Aquaporin-4 deletion in mice reduces brain edema after acute water intoxication and ischemic stroke., Nat. Med. 6 (2000) 159–163. doi:10.1038/72256.

[113] S. Eriksson, K. Elbing, O. Söderman, K. Lindkvist-Petersson, D. Topgaard, S. Lasič, NMR quantification of diffusional exchange in cell suspensions with relaxation rate differences between intra and extracellular compartments, PLoS One. 12 (2017) 1–

18. doi:10.1371/journal.pone.0177273.

[114] C. Badve, A. Yu, M. Rogers, D. Ma, Y. Liu, M. Schluchter, J. Sunshine, M. Griswold, V. Gulani, Simultaneous T1 and T2 Brain Relaxometry in Asymptomatic Volunteers Using Magnetic Resonance Fingerprinting, Tomography. 1 (2015) 136–144. doi:10.18383/j.tom.2015.00166.

[115] Y. Ohene, I.F. Harrison, P. Nahavandi, O. Ismail, E. V. Bird, O.P. Ottersen, E.A. Nagelhus, D.L. Thomas, M.F. Lythgoe, J.A. Wells, Non-invasive MRI of brain clearance pathways using multiple echo time arterial spin labelling: An Aquaporin-4 study, Neuroimage. (2018). doi:10.1016/J.NEUROIMAGE.2018.12.026.

[116] X. Shao, S.J. Ma, L. Cao, M. Casey, J.M. Ringman, D.J. Wang, Measuring Water Exchange Across Blood Brain Barrier in Elderly Subjects By Diffusion Weighted Pseudo-Continuous Arterial Spin Labeling, Alzheimer's Dement. 14 (2018) P835–P836. doi:10.1016/j.jalz.2018.06.1060.

[117] P.W. Hales, C. a Clark, Combined arterial spin labeling and diffusion-weighted imaging for noninvasive estimation of capillary volume fraction and permeability-surface product in the human brain, J. Cereb. Blood Flow Metab. 33 (2012) 67–75. doi:10.1038/jcbfm.2012.125.

[118] Z. Lin, Y. Li, P. Su, D. Mao, Z. Wei, J.J. Pillai, A. Moghekar, M. van Osch, Y. Ge, H. Lu, Non-contrast MR imaging of blood-brain barrier permeability to water, Magn. Reson. Med. 80 (2018) 1507–1520. doi:10.1002/mrm.27141.

Glossary of abbreviations

ASL – arterial spin labelling

AD – Alzheimer's disease

AQP1/AQP4 – aquaporin water channels 1 and 4

BBB - Blood brain barrier

CAPTIVE – Continuous assessment of perfusion by tagging including volume and water extraction

CBF – cerebral blood flow

CBV – cerebral blood volume

DCE-MRI – dynamic contrast enhanced MRI

EPI – echo planar imaging

GLUT1 – Glucose transporter 1

IDEALS – Intrinsic diffusivity encoding of arterial labelled spins

IR – inversion recovery

IVIM – Intravoxel incoherent motion

MCAo – middle cerebral artery occlusion

MFAME-MRI – multi-flip angle multi echo MRI

MS – multiple sclerosis

NMR – nuclear magnetic resonance

PET – positron emission tomography

PLD – post-labelling delay

PS – permeability surface area product

PSF – point spread function

RARE – Rapid imaging with refocussed echoes

SNR – signal to noise ratio

SPA – single pass approximation model

SPGR – spoiled gradient echo

SPION – Super paramagnetic iron oxide nanoparticle

SSS – superior sagittal sinus

TR – repetition time

TE – echo time

TJ – tight junction

WEI –water exchange index

DW-MRI – Diffusion-weighted MRI

OSA – obstructive sleep apnea